AD-A113 894 NAVAL UNDERWATER SYSTEMS CENTER NEW LONDON CT NEW LO--ETC F/G 14/5
PREDICTION OF OPTICAL IMAGE QUALITY NEAR THE SEA SURFACE FROM M--ETC(U)
JAN 82 F S REPLOGLE, C W FAIRALL

UNCLASSIFIED NUSC-TM-821008 NL

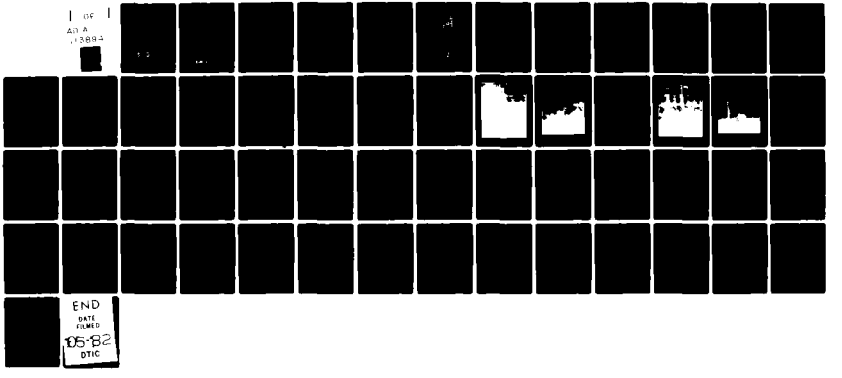

END
DATE FILMED
05-82
DTIC

TM No. 821008

(1)

AD A113894

NAVAL UNDERWATER SYSTEMS CENTER
New London Laboratory
New London, Connecticut 06320

Technical Memorandum

PREDICTION OF OPTICAL IMAGE QUALITY NEAR THE SEA SURFACE FROM METEOROLOGICAL MEASUREMENTS

Date: 25 January 1982

Prepared by: F. Replogle, Jr.
F. Replogle, Jr.
Submarine Electro-Optics
Division

C. W. Fairall
C. W. Fairall
BDM Corporation
Naval Postgraduate School
Monterey, California

Approved for Public Release: Distribution Unlimited

BLANK PAGE

ABSTRACT AND SUMMARY

This report presents a mechanism for calculation of the optical index structure constant C_n^2 from bulk meteorological measurements (air and water temperatures, wind speed, air humidity) made over the ocean. From this and a formulation of the near field optical propagation from an incoherent point source, the expected line spread function for near the sea surface lines of sight is calculated. Finally, three series of photographic line width observations, made during unstable, neutral, and stable atmospheric buoyancy conditions, are compared with line widths expected from the calculations. Mean values of observed results agree with the calculations within about 25 percent for conditions of strong atmospheric instability. Since comparisons were made over a variety of target ranges, wind speeds, and camera elevations, it is concluded that the formulations derived are accurate to at least ± 25 percent for conditions of strong atmospheric instability.

The observations made under conditions of neutral and stable atmospheric buoyancy were instrumentally limited to an angular subtense of 2 to 4 arc seconds. These measured line width values fall between 1.9 and 0.6 times the values computed from meteorological measurements.

The variability of image spreading observed across the target fields points out the difficulty of employing a single mechanism for correction of atmospherically induced image smear.

ADMINISTRATIVE INFORMATION

This work was performed under NUSC Project No. A50040, "Periscope MTF Study--Refractive Irregularity Portion," Principal Investigator, F. S. Replogle, Jr. (Code 3422); Program Element 61152N, Navy Subproject/Task No. ZR 000 01 01, "Independent Research," Program Managers, J. H. Probus and D. F. Parrish, Naval Material Command (MAT 08T1 and 08L).

The work was a cooperative effort with personnel from the Physics and Meteorology Departments of the Naval Postgraduate School of Monterey, California. Assistance of Naval Postgraduate School personnel was furnished to the Naval Underwater Systems Center without charge.

Author Replogle is located at the New London Laboratory, Naval Underwater Systems Center, New London, Connecticut 06320. Author Fairall formerly employed directly by the Naval Postgraduate School, Monterey, California, now serves there as an employee of BDM Corporation.

I. INTRODUCTION AND BACKGROUND

The information collection capability of photography with a camera located near the sea surface is limited by the luminance characteristics of the target, by the characteristics of the atmospheric path, and by the characteristics of the camera in its local environment. Significant losses of information arise from the loss of contrast and picture smearing resulting from the characteristics of the atmosphere along the line-of-sight. Relationships predicting the loss of contrast are relatively well known;[1] however, the relationships between picture smearing (attenuation of optical modulation transfer), sea state, height of the line-of-sight above the surface, and meteorological parameters have only recently been developed. In particular, the formulation of the relationship of the strength of the turbulence C_n^2 to gross meteorological parameters in the near-the-ocean-surface environment has been under development only since 1974,[2] and no measurements of C_n^2 have been made closer than one meter from the sea surface. This independent research effort is one of the first which relates meteorological variables, turbulence, and picture smearing for a near-the-ocean line of sight. The ultimate goal is to be able to predict the smearing due to turbulence, given details on the camera and target geometries and the gross meteorology at a particular site.

In a previous NUSC effort[3] the recording camera was located in a tent on a beach. The target was mounted on a ship stationed from 2 to 3.7 km. away. The effective turbulence level for the integrated line of sight was much larger than the turbulence level measured strictly over the water. The result was attributed to turbulence generated by breakers and by the shore.

In the current effort, the camera equipment was located on an offshore tower to provide a full over-water line of sight, and meteorological measuring equipment was located nearby (c.f. Fig. 1). The meteorological measurements performed for this study include primarily macro (bulk) meteorological measurements. A few micro meteorological measurements were obtained for use in comparison calculations of C_n^2.

In this memorandum a mechanism for deriving values of the index structure constant, C_n^2, from values of bulk meteorological parameters is presented.* From this, using near field optical propagation formulations, expected values of the width of the optical line spread function for incoherent imaging are obtained. These are compared with averages of measured line spread function widths. Criticisms of experimental results and conclusions follow.

The meteorological portion of the study was guided by personnel of the Meteorology and Physics Department of the Naval Postgraduate School of Monterey, California. Measurements of variables, data reduction, and optical propagation portions of the study were carried out by NUSC personnel.

II. TURBULENCE THEORY

a. Structure Functions

In the nature of turbulence produced by shear flow, the initial power input is into large eddies. This power is then transferred from large to

* Details of the approach have been given by Davidson, et alia, in Reference 4.

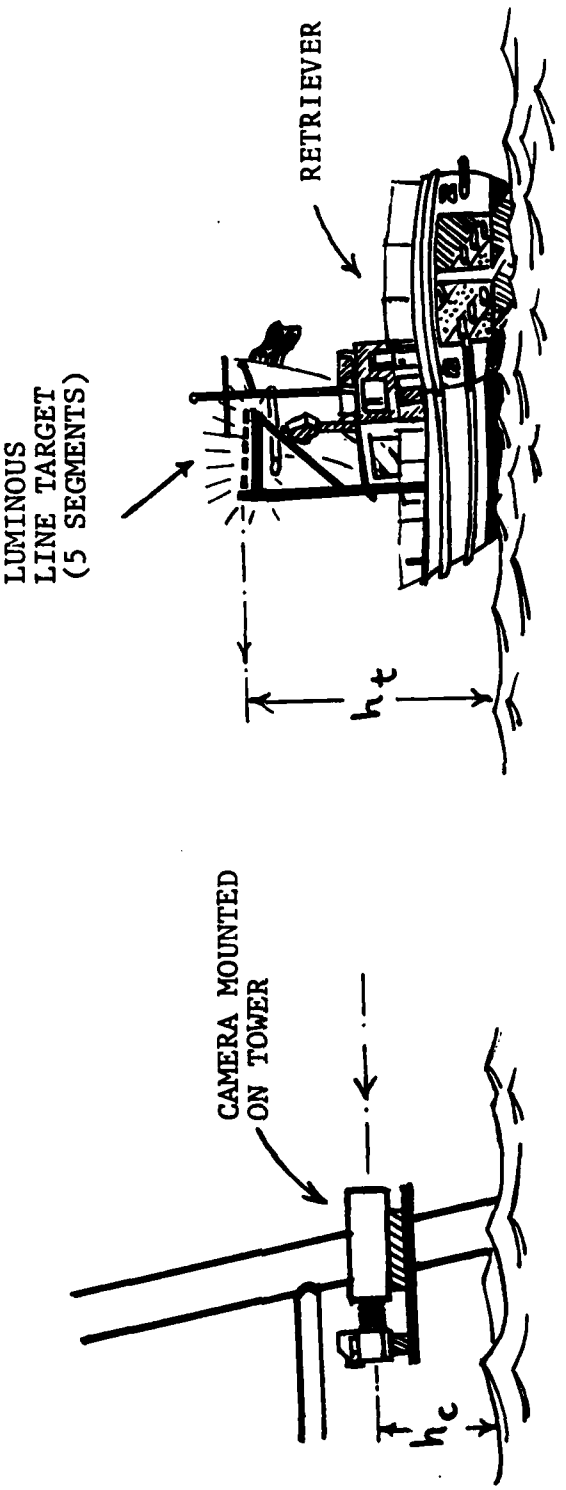

FIGURE 1

SCHEMATIC ILLUSTRATION OF GEOMETRY USED IN TAKING OPTICAL DATA

smaller eddies with little energy loss until it is finally converted into heat by viscous forces when the eddy sizes approach the inner scale of turbulence l_0 (with dimensions of a few mm.). When the shear is produced by friction in flow parallel to a boundary, the scale size L_0 of the input eddies at a distance z from the boundary is approximately equal to z. For distances r lying in this inertial range, i.e., $L_0 > r > l_0$, we may define a velocity structure function D_V giving the mean square velocity V difference for two points separated by a distance r,

$$D_V(|\vec{r}|) = \langle [V(\vec{0}) - V(\vec{r})]^2 \rangle, \tag{1}$$

where for simplicity the definition is expressed in scalar fashion,* and where over distances of the order of r, the turbulence is isotropic. For distances r within the inertial range, the Kolmogoroff or Von Karman spectrum of turbulence element sizes leads to the relationship:

$$D_V(r) \sim r^{2/3} \tag{2a}$$

It has been shown that when gradients of passive additive elements, e.g., temperature θ or humidity Q, exist in the shear flow, the spectra of element sizes lead to similar relationships, i.e.,

$$D_\theta(r) = C_\theta^2 \cdot r^{2/3} \tag{2b}$$

and

$$D_Q(r) = C_Q^2 \cdot r^{2/3} \tag{2c}$$

respectively, where the proportionality constants C are "constant" over regions having dimensions of the order of fractions of meters, but may vary slowly over larger distances. Since the changes in optical index n are related to air density and humidity changes, we have a similar relationship for this variable

$$D_n(r) = C_n^2 \cdot r^{2/3}. \tag{3}$$

C_n^2 has been called the optical index "structure parameter."

---

* Properly used, D_V is a second rank tensor.

b. General Macrometeorological Relationships

For calculations of the strength of the optical structure parameter C_n^2 from bulk meteorological parameter measurements, the following input variables are used:

z = height above ocean surface (m.)
$T(z)$ = air temperature (^oK.)
T_o = water surface temperature (^oK.)
$q(z)$ = humidity mixing ratio (gms. water/kg. air)
q_o = humidity mixing ratio at sea surface (100% r. h. at $T = T_o$)
$U(z)$ = wind speed (m./sec.)
P = atmospheric pressure (millibars)

From these one uses the functions:

$\theta(z)$ = potential temperature = $T(z) + .01z$
$\Delta(z) = (z) - T_o$
$\Delta q(z) = q(z) - q_o$
$\xi = z/L$

where

L = Monin-Obukhov scaling length (m.)

is a constant obtained from formulations of $\Delta\theta$, ΔQ, and U.

Since the formulations to be used differ markedly with the convective stability of the atmosphere, we proceed to define stability by

$\Delta\theta(z) + 6.1 \times 10^{-4} T(z)\, \Delta q(z) > 0$: stable atmosphere
$\Delta\theta(z) + 6.1 \times 10^{-4} T(z)\, \Delta q(z) < 0$: unstable astmosphere
$\Delta\theta(z) + 6.1 \times 10^{-4} T(z)\, \Delta q(z) = 0$: neutral atmosphere

Following the approach of Ref. 4, it is then possible to utilize values of T, T_o, q, U and P measured at a height of convenience (e.g. 5 to 20 m.) to obtain a continous formulation giving $C_n^2(z)$. The necessary steps are outlined in Appendix I. The resulting expression is

$$C_n^2 = 6.2\times10^{-9} \cdot P^2 \cdot T^{-4} \cdot \left[T_*^2 + 0.070 T_* Q_* + 0.0019 Q_*^2\right] z^{-2/3} f(z/L), \qquad (4)$$

where P is pressure in mb
T is absolute temperature
T_*, Q_* and L are computed in accordance with Appendix I

$$f(z/L) = 4.9\,[1+2.4\,(z/L)^{2/3}] \text{ for a stable atmosphere} \qquad (5.a)$$

and

$$f(z/L) = 4.9\,[1-7\,z/L]^{-2/3} \text{ for an unstable atmosphere} \qquad (5.b)$$

With this formulation, we proceed to determining the effect of C_n^2 upon imaging over a slant path above the sea surface.

III. OPTICAL PROPAGATION AND IMAGING THEORY

a. Effective Refractive Irregularity Strength Over the Line of Sight

To treat the propagation of imaging light from the target to the camera in the optical "near field,"* we assume that the target consists of a series of incoherent point sources of spatially varying intensity. Imaging light from each source then acts independently and travels through the turbulent medium to a camera at a range R. With a point source, turbulence elements affect the image in accordance with the 5/3 power of the distance from the source.[4,5] Thus, the effective product of the refractive irregularity strength and the path length becomes:

$$C_n^2(\text{eff})\cdot R = \int_0^R C_n^2\,(x)\cdot(x/R)^{5/3}\cdot dx, \tag{6}$$

where x is the distance from the source. To simplify our analysis, we assume that the turbulence is uniform over the range, i.e., the turbulence is statistically uniform at any particular height h above the water, but the average value varies with h, or

$$C_n^2(\text{eff})\cdot R = \int_0^R C_n^2\,[h(x)]\cdot(x/R)^{5/3}\cdot dx. \tag{7}$$

In terms of the geometry of Figure 1,

$$h = h_t - x(h_t - h_c)/R = h_t(1 - \alpha x/R), \tag{8}$$

where

h_t = height of target
h_c = height of camera
$\alpha = 1 - h_c/h_t$.

For the case of a stable atmosphere, if we use Equations (4) and (5.a) the height dependence of C_n^2 may be expressed by

$$C_n^2(h) = C_n^2(h_m)\cdot\left[\left(\frac{h_m}{h}\right)^{2/3} + 2.4\left(\frac{h_m}{L}\right)^{2/3}\right]\Big/\left[1 + 2.4\left(\frac{h_m}{L}\right)^{2/3}\right], \tag{9}$$

---

* In the "near field" of optical propagation wavefront distortions of the receiver are primarily optical phase distortions; whereas in the "far field" optical amplitude distortions, leading to image scintillation, also occur.

where h_m is the height at which C_n^2 is measured or derived from bulk meteorological measurements. Substituting C_n^2 from Equation (9) in Equation (7) and letting $x/R = u$ gives:

$$C_n^2(\text{eff}) \cdot R = \frac{R \cdot C_n^2(h_m) \cdot h_m^{2/3}}{[1 + 2.4(h_m/L)^{2/3}]} \cdot \left[\frac{2.4}{L^{2/3}} \cdot \int_0^1 u^{5/3} du + \frac{1}{h_t^{2/3}} \cdot \int_0^1 \frac{u^{5/3} du}{(1 - \alpha u)^{2/3}}\right]$$

$$= \frac{R \cdot h_m^{2/3} C_n^2(h_m)}{[1 + 2.4(h_m/L)^{2/3}]} \cdot \left[\frac{0.9}{L^{2/3}} + \frac{1}{h_t^{2/3}} \cdot I(\alpha, 0)\right], \tag{10}$$

where the function:

$$I(\alpha,\beta) = (1 + 7\beta)^{2/3} \cdot \int_0^1 \frac{u^{5/3} du}{\{(1 - \alpha u)\,[1 + 7\beta(1 - \alpha u)]\}^{2/3}}, \tag{11}$$

with

$$\alpha = 1 - h_c/h_t$$
$$\beta = -h_t/L,$$

is given by the graph of Figure 2.

For the case of an unstable atmosphere, Equations (4) and (5.b) give the height dependence of C_n^2 as:

$$C_n^2(h) = C_n^2(h_m) \cdot \left[\frac{h_m(1 - 7h_m/L)}{h(1 - 7h/L)}\right]^{2/3}. \tag{12}$$

Substituting for h from Equation (8) in Equation (12) and also Equation (12) in Equation (7) gives for $C_n^2(\text{eff}) \cdot R$

$$C_n^2(\text{eff}) \cdot R = R \cdot C_n^2(h_m) \cdot \left[\frac{h_m(1 - 7h_m/L}{h_t(1 - h_t/L)}\right]^{2/3} \cdot I(\alpha,\beta). \tag{13}$$

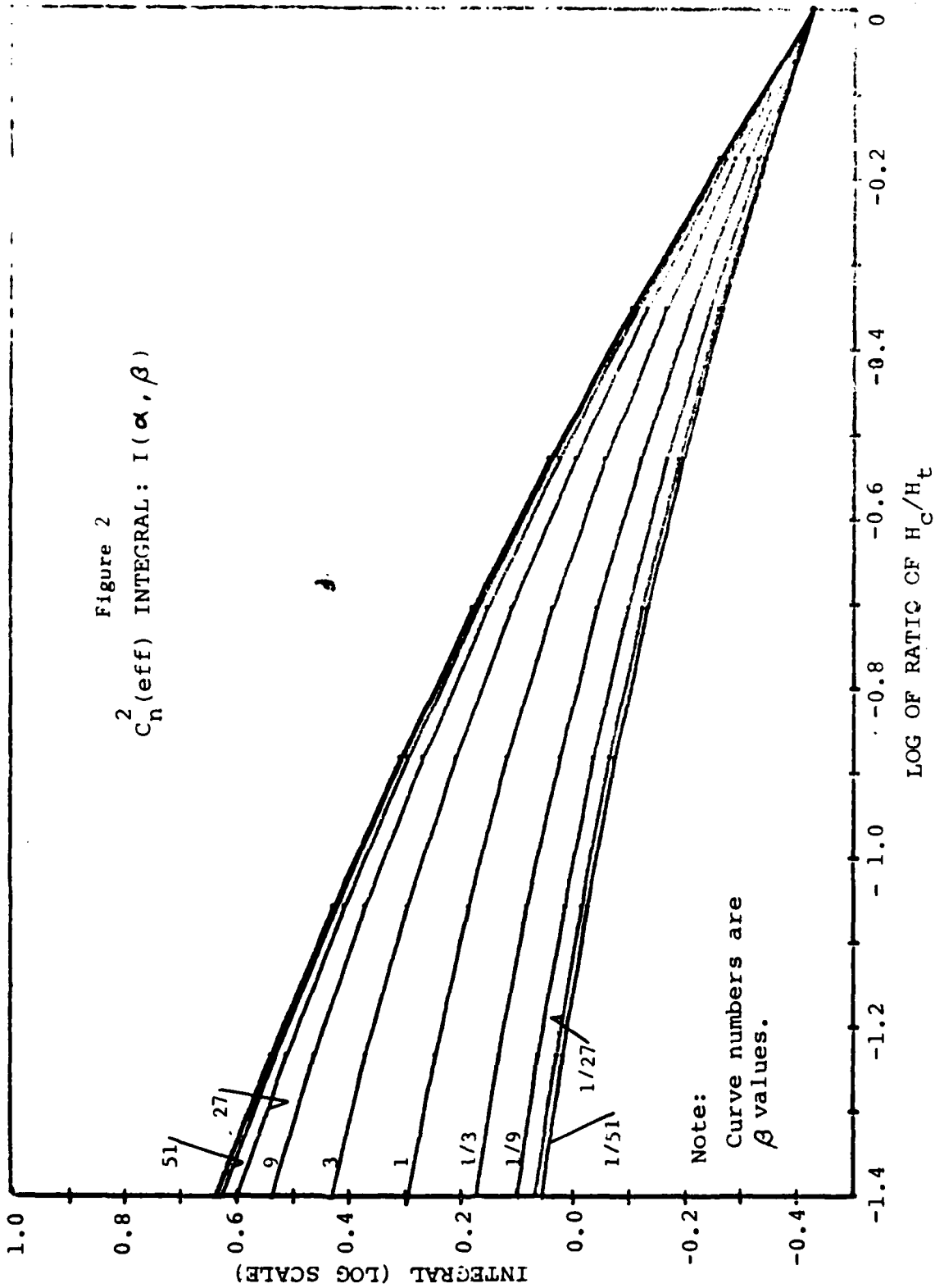

Figure 2
C_n^2(eff) INTEGRAL: $I(\alpha, \beta)$

Values of $I(\alpha, \beta)$ may be obtained similarly from the curves of Figure 2.

b. Mutual Coherence Function

Yura[7] gives an expression for the averaged mutual coherence function (MCF) of light from an incoherent point source propagated through a turbulent atmosphere to an aperture of diameter D as:

$$M_{st}(\rho,R) = \exp\left\{-(\rho/\rho_0)^{5/3}\left[1 - \delta\cdot(\rho/D)^{1/3}\right]\right\} \qquad (14.a)$$

where

M_{st} = the averaged short term (short exposure) MCF

ρ = $\lambda f F$ = wavelength·camera focal length·spatial frequency in image plane

ρ_0 = long term (long exposure) coherence distance

$$= \left[\frac{2.91}{2}\cdot C_n^2(\text{eff})\cdot\left(\frac{2\pi}{\lambda}\right)^2\cdot R\right]^{-3/5}$$

$$= \left[1.60 \times 10^{-14} C_n^2(\text{eff})\cdot R\right]^{-3/5} \qquad (14.b)$$

λ = 6×10^{-7} m. (approx.)

δ = multiplier in the range from 0.5 to 1.0 depending upon the target range. 0.5 corresponds to far field imaging; 1.0 corresponds to near field imaging.* In our case, we used the multiplier 0.75 in all the calculations, except in the 1980 series. Since the atmosphere was neutral then, imaging was near field, and δ = 1.0.

c. Camera Line Spread Function

Equation (14.a) is also in the form of a statistically-averaged modulation transfer function MTF for the cone of atmosphere from the receiving aperture to a target point. To obtain the MTF for the full recording system MTF_{sys}, we multiplied the atmospheric response by the (approximated) frequency response H of an ideal telescope having an 86 mm window and a 25 mm obscuration and by an approximation to the frequency response J of Pan-X film obtained from a handbook graph. Then substituting the value 6×10^{-7}m for λ and 1.47 m for f gives for the overall response

$$MTF_{sys}(F,\rho_0) = \exp[-8.8 \times 10^{-7}\cdot(F/\rho_0)^{5/3}\cdot(1 - 0.0219\ \delta.F^{1/3})]\cdot H(F)\cdot J(F), \qquad (15)$$

where $\rho_0(C_n^2,R)$ was defined in Equation (14.b),

* If $\rho_0 << \lambda R$, imaging is far field. If $\rho_0 >> \lambda R$, imaging is near field.

$$H = F/60{,}000 \quad \text{if } 0 < F \leq 30{,}000$$
$$H = 1.0/1.4 - F/140{,}000 \quad \text{if } 30{,}000 < F \leq 100{,}000$$
$$H = 0 \quad \text{if } F > 100{,}000$$

and

$$J = [1 + 3(F/53{,}000)^2]^{-1/2},$$

where the units of F are cycles/m.

To compare empirical with theoretical results, one might Fourier transform the observed image spread functions and compare the averaged transforms with Equation (15). Rather than perform the multiplied measurements and transforms which this would require, we Fourier transformed Equation (15) to obtain expected average line spread functions for a variety of ρ_0 values and for δ = 0.75 and 1.0. Figure 3 gives smoothed curves showing the values of line widths (1/e times peak amplitude) obtained from these transforms. These were used for determining expected line widths.

IV. EXPERIMENTAL ARRANGEMENT

The line of sight from the target to the camera was as shown in Figure 1. The camera, a "Questar" telescope coupled to a Nikon 35 mm. camera back, was attached to a tower corner post at a variety of heights h_c above mean water level. The target consisted of a series of five 1000 watt quartz-iodide bulbs, each having a luminous area of 160 by 1.0 mm. The target was placed at a variety of heights h_t at ranges R from 460 to 5000 m.

The meteorological measuring equipment was located on an adjacent corner of the tower in the 1978 observation series and on a mast rigged on the bow of the freighter YFRT-287 in the 1980 and 1981 observation series. The freighter was anchored 460 m from the tower, just downwind from the camera's line of sight. The equipment consisted of an anemometer, wind vane, dew point apparatus, air-water temperature difference measuring apparatus, and water temperature measuring apparatus. The in-air sensors were located 5.7 m. above the water level in the 1978 series and 7.0 and 8.1 m. above the water level in 1980 and 1981. Water temperature measurements were of the "bucket" variety.

In the 1980 observation series, a micrometeorological (differential air temperature measuring) apparatus* and recorder were mounted on the Brenton Reef Tower. By means of differential temperature measurements made by this instrument in the air stream, values for the temperature structure function of the air could be obtained directly. And these were simply convertible to the optical index structure function which was needed for describing and calculating optical image propagation. This apparatus was used on the data taking effort of 16 May, 1980. The results obtained from this apparatus were compared with values of C_n^2 deduced from simultaneously-made bulk meteorological measurements. When we attempted to use the micrometeorological measuring apparatus on the primary data taking exercise of 6 June, 1980, the fragility of the probes and the lack of a sufficient number of spares limited our data taking to four single measurements.

* Contel, Inc., Model MT-2 microthermal probe

FIGURE 3

THEORETICAL MEAN LINE WIDTH VALUES FOR NEAR AND INTERMEDIATE FIELD PROPAGATION

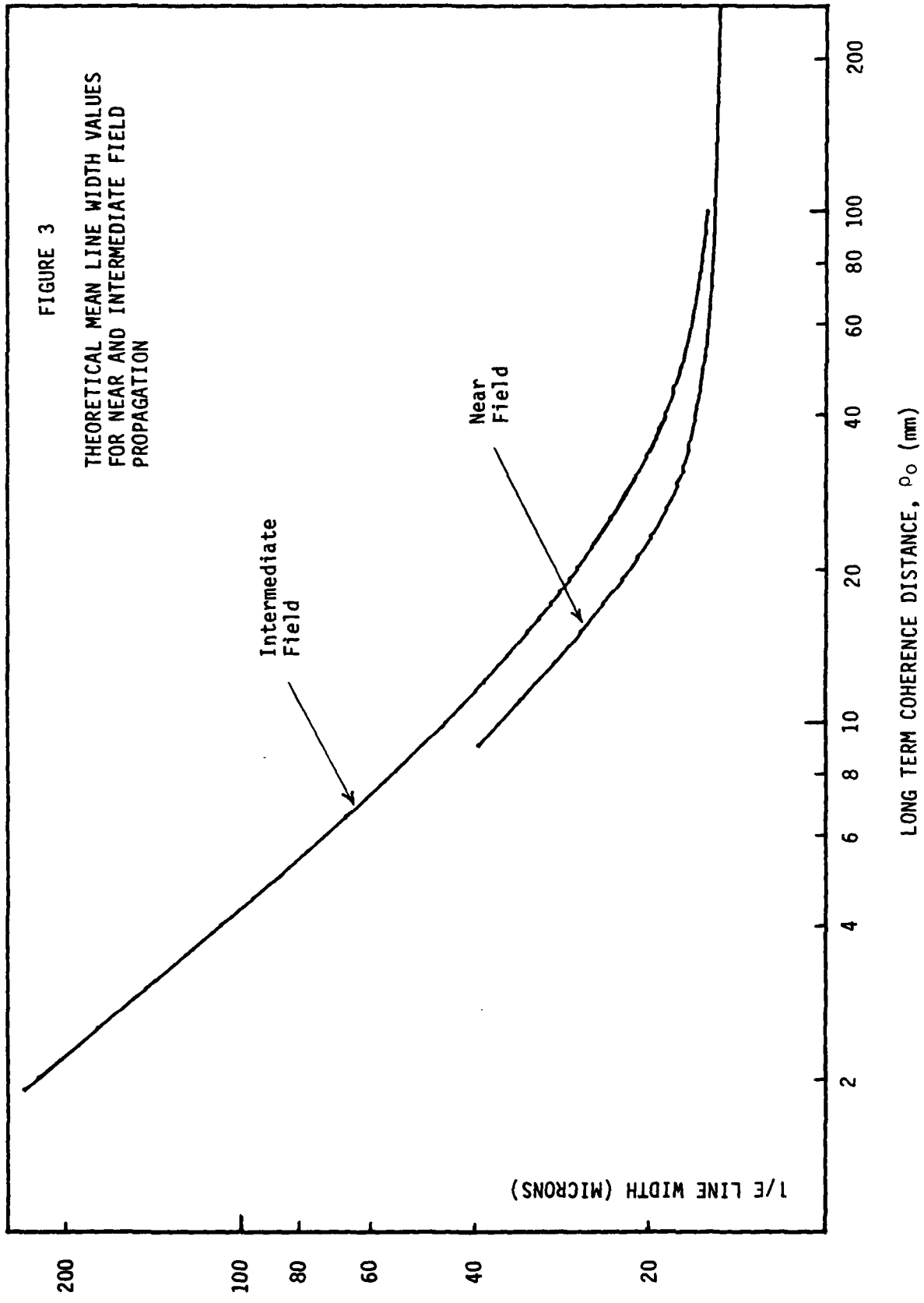

Unfortunately, the air-water differential temperature apparatus and the micrometeorological apparatus failed to operate in the 1981 data taking series. The air-water differential temperature apparatus was replaced with a thermometer located on the shady side of the ship's mast and a thermometer kept in a bucket in the water.

Accuracy limitations of the sensors were approximately as follows:

Static camera resolution (with Pan-X film)	2.5 arc sec. (equiv. to 18 microns on the film)
Image smearing due to target motion	0.04 arc sec., max., in 1/250 sec. exposure
Luminous target geometrical line width	0.45 arc sec., max.
Wind speed	0.5 m/sec. starting speed; running accuracy ± 0.5 m/sec.
Dew point temperature	± 1°C
Air-water differential temperature (air sensor is aspirated and double-shielded in 1978 and 1980 series)	± 0.1°C (est) for 1978 and 1980 series ± 0.5°C (est) for 1981 series
Water temperature measuring apparatus	± 1°C
Differential air temperature measuring apparatus	± 10^{-17} C_n^2 units

V. DATA TAKING AND PROCESSING

a. General

The three series of observations were made at Brenton Reef Tower, located just off the entrance to Narragansett Bay, R.I. The tower's location vs. the nearest land is shown on the map of Figure 4. We attempted to position the target carrying ship in a direction such that the camera line of sight was normal to the wind direction. Camera-target heights and ranges are given in Table I. In nearly all cases the camera exposure time was 1/1000 sec. To ascertain that critically-focussed images were obtained, we first determined the relationship between the camera viewer best focus and the film best focus positions in the laboratory. Then in the field, at every target range recordings were made for a series of focus positions bracketing the laboratory-determined best focus position.

TABLE I

GEOMETRY FOR FILM RECORDING

Observation Series	Day	Time	Target Ranges (m)	Target Height (m)	Mean Camera Height (m)
A	9/26/78	10:00-11:30	460-2740	6.2	2.4
B	9/26/78	11:45-12:50	460-2740-460	6.2	1.4
C	9/26/78	14:00-14:30	460-1830	6.2	1.0
F	9/27/78	12:30-12:50	2740-460-1830	6.2	2.3
G	9/27/78	13:25-14:00	460-2740-460	6.2	0.8
H	6/6/80	10:55-13:05	990-4970-520	9.85	0.9
I	6/6/80	14:05-15:40	950-5145-500	9.85	1.7
J	6/6/80	16:00-17:15	425-5030-1000	9.85	3.1
K	5/8/81	10:05-11:18	500-4000-3000	7.9	1.1
L	5/8/81	11:30-12:15	5000-500	7.9	0.95
M	5/8/81	12:35-14:02	500-5000-500	7.9	2.0
N	5/8/81	14:30-15:00	500-5000	7.9	3.3

Bulk meteorological data were taken and recorded continuously during the three expeditions. Recorded results were first averaged for fifteen or thirty minute periods; then the averages were interpolated to give data for the camera image recording times.

In the laboratory the ends of each exposed film strip were given a step wedge exposure, and the film was processed continuously in a Versamat processor. Then by use of a microscope and scale, the image negatives were scanned to determine approximate image widths and thus to determine the best-focus frames. These were then scanned with a Joyce-Loebl Model 3C micro-densitometer.* On the selected frames we attempted to choose nominally average portions of the five source images for scanning. This same principle

* The formulation $[(\text{measured width})^2 - (\text{scanning slit width})^2]^{1/2}$ was used as a correction factor for the image broadening caused by finite slit width.

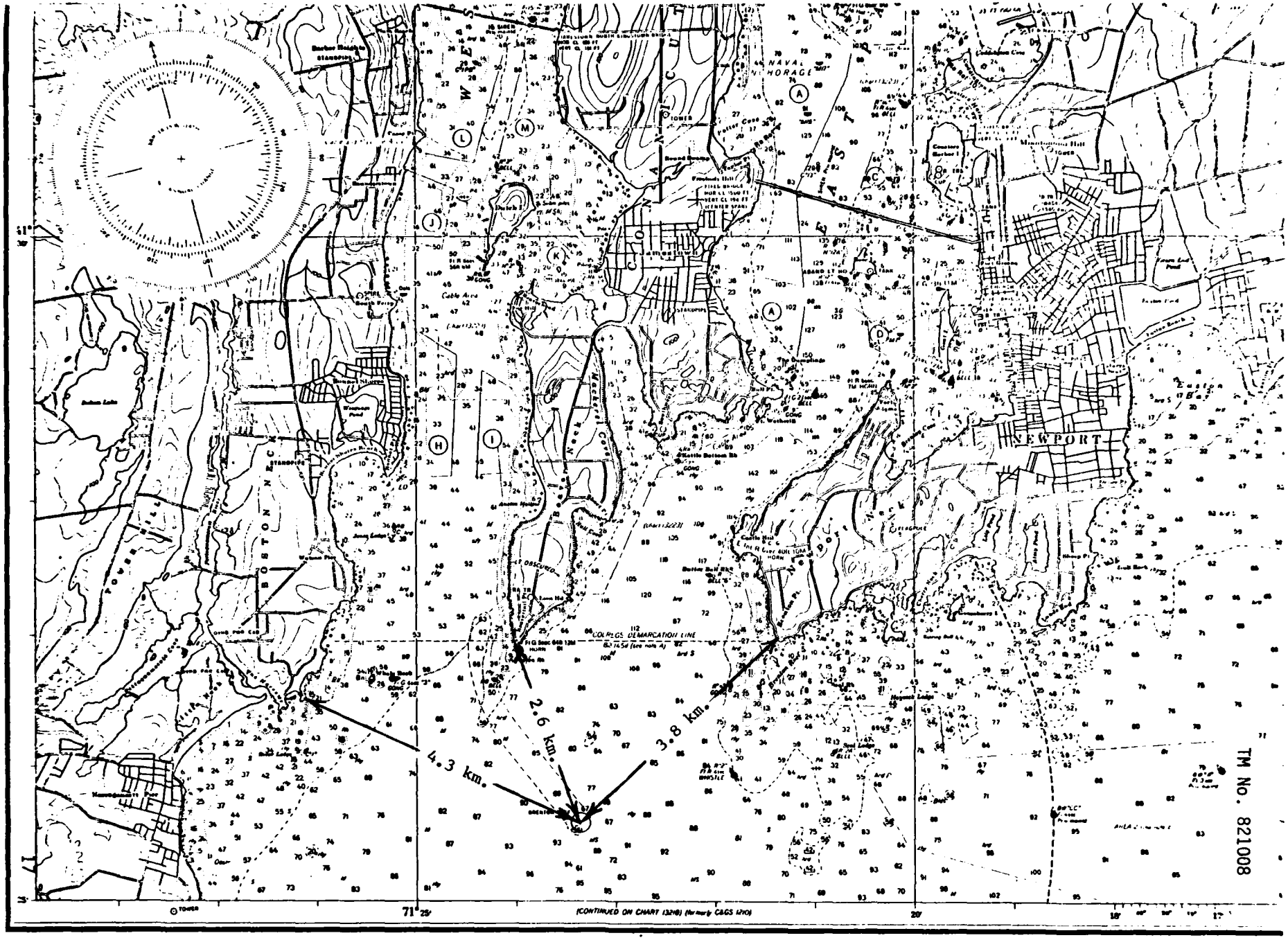

13221

FIGURE 4 LOCATION OF BRENTON REEF TOWER AT ENTRANCE TO NARRAGANSETT BAY
WATER DEPTHS ARE IN FEET

was applied when the images were smeared together because of atmospheric irregularities. On any scan the peak density value was obtained from a (visually) smoothed trace, and an averaged background density value was obtained. From the step wedge exposures, the density vs exposure transfer (H and D) curve for Pan-X film was obtained, and the equivalent peak and background exposures E_p and E_b were found. Then the 1/e'th signal exposure level E_{es} was calculated from

$$E_{es} = (E_p - E_b)/e, \tag{16.a}$$

and the corresponding exposure with background added was

$$E_e = E_p/e + E_b(1 - 1/e). \tag{16.b}$$

By the use of the transfer curve again, the image density corresponding to E_e was determined. Then the image width between 1/e'th points was measured. Finally, for a particular exposure series and target range, the 1/e image widths were averaged to obtain mean values, and expected standard deviations of the mean and of individual images were computed.

b. 1978 Observation Series

The first series of observations was made with a strongly unstable marine atmosphere on September 26 and 27, 1978. Thirty minute averages of the recorded meteorological data are shown on the eight lower curves of Figures 5a and 5b. On September 26 the sky was fully clear. The uppermost curves give values of C_n^2 computed by Naval Postgraduate School personnel for the meteorological apparatus height, 5.7 m.

On this expedition, a total of 411 exposures were made, and line widths were measured on 73 of these. Figures 6 and 7 are enlarged prints of "typical" exposures from Series A. By use of a mask the light source portions of the negatives were overprinted to show the structure in the spread functions. Since the exposure times for the negatives were chosen to avoid saturation of the target source portion of the frame, the ship and background are underexposed. The length of the target array is 0.8 m.

c. 1980 Observation Series

On the expedition of 16 May, 1980, the shutter of the Nikon data camera failed to operate, resulting in no film exposures. Thus, only micro-meteorological and bulk meteorological measurements obtained on this date were useful. Figure 8 compares values of C_n^2 computed from bulk meteorological measurements with values obtained by means of the microthermal bridge apparatus.

The major results of the series were obtained on the expedition of 6 June, 1980. At this time, about 460 exposure (images of the target) were made, and 98 of these were scanned subsequently with the laboratory's micro-densitometer. Each exposure was scanned about three times to obtain a mean value for the spread of the line image on the frame. 37 of these frames were then selected as representative of best focus conditions, and from these the line widths representative of the geometrical conditions of the data taking were obtained. Figures 9 and 10 are representative photographs of targets at 1000 and 4970 m. The quality of the target image in Figure 10 should be compared with the image of Figure 7 obtained in the presence of strong turbulence at only 1830 m. range.

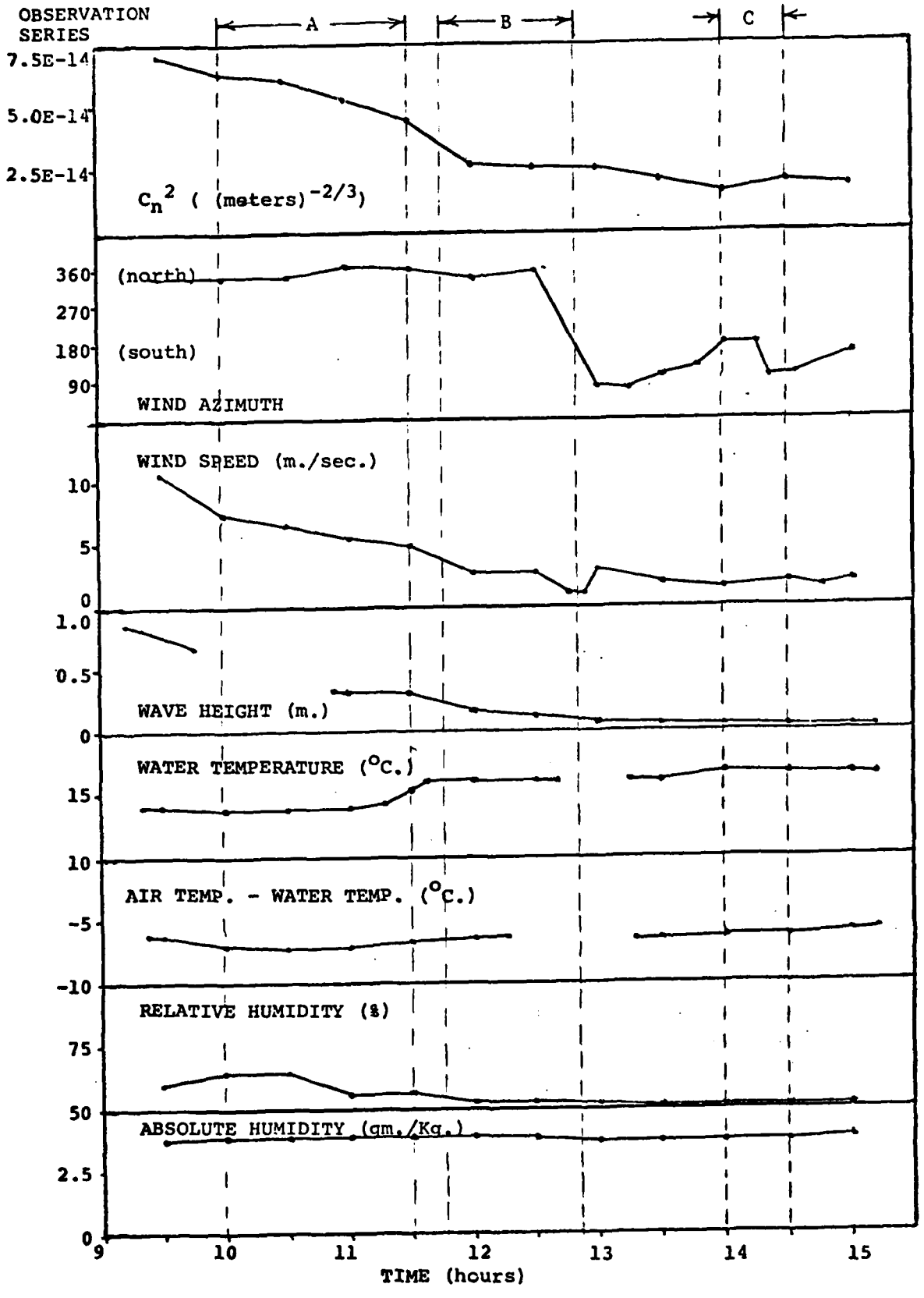

Figure 5.a METEOROLOGICAL DATA TAKEN ON SEPTEMBER 26, 1978 AND RESULTING COMPUTED VALUES OF C_n^2

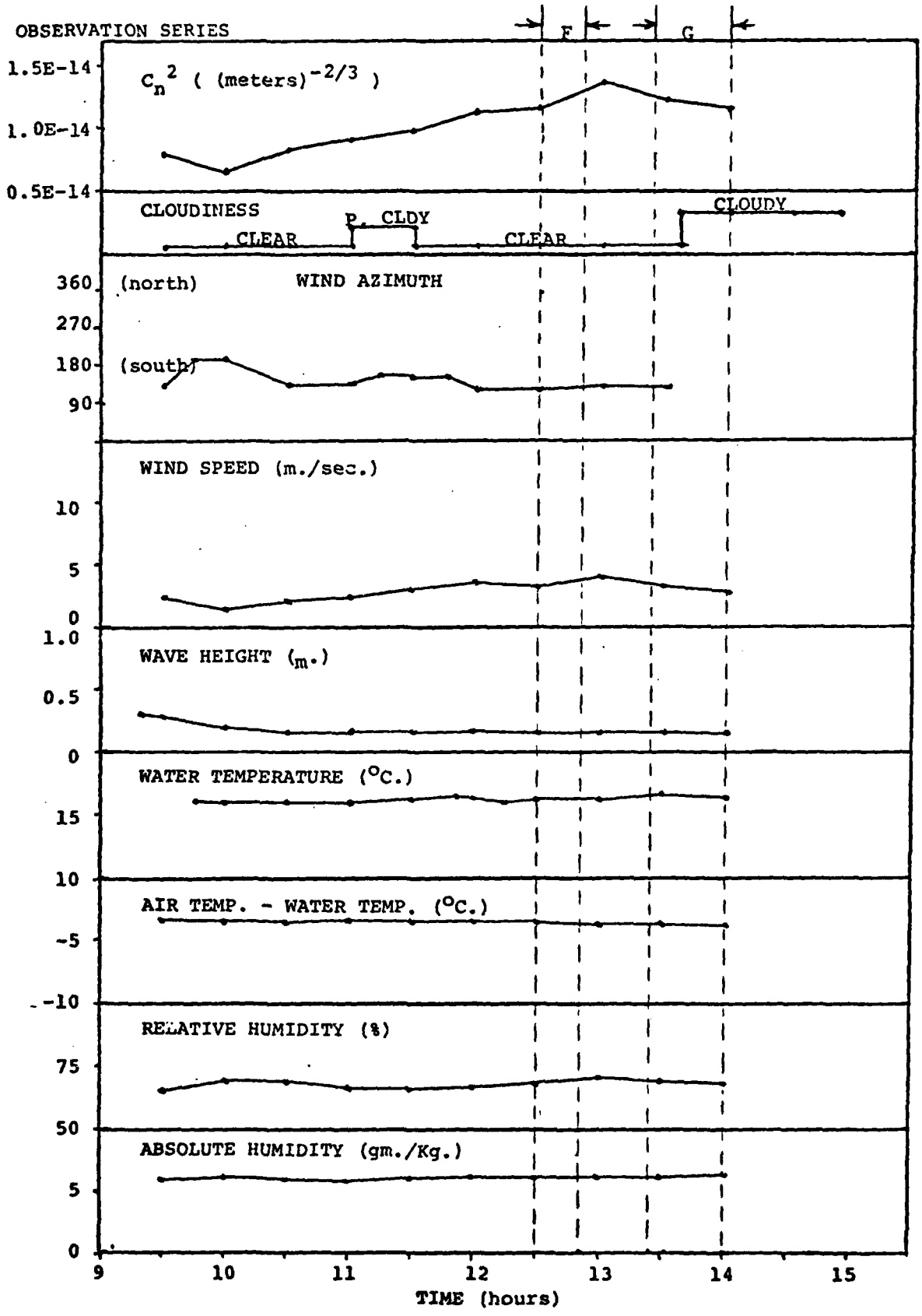

Figure 5.b METEOROLOGICAL DATA TAKEN ON SEPTEMBER 27, 1978 AND RESULTING COMPUTED VALUES OF C_n^2

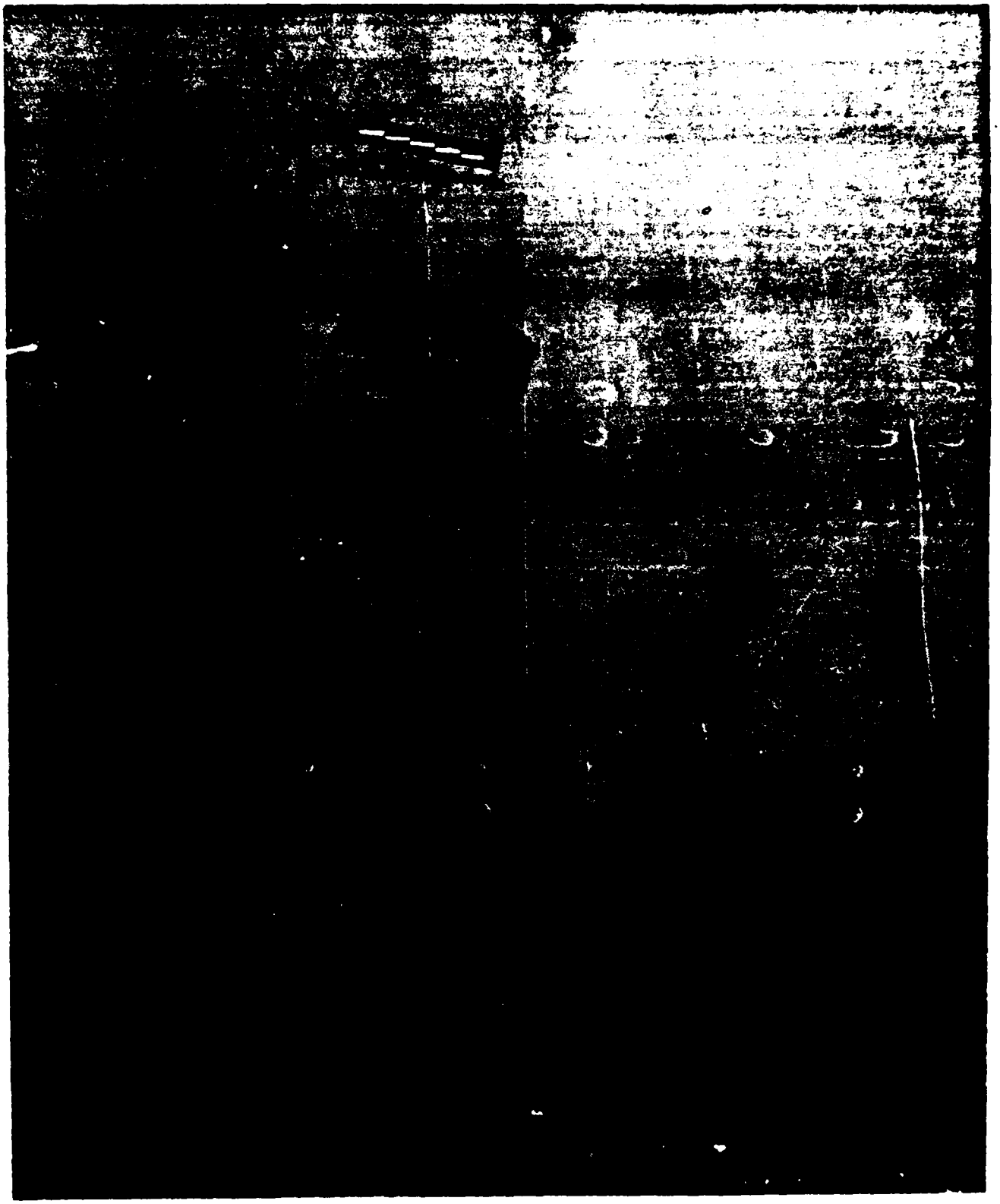

FIGURE 6 ENLARGED PRINT OF IMAGE OBTAINED WITH A STRONGLY TURBULENT ATMOSPHERE
Range: 460m.; C_n^2: 6.4 X 10^{-14}

FIGURE 7 ENLARGED PRINT OF IMAGE OBTAINED WITH A STRONGLY TURBULENT ATMOSPHERE
Range: 1830 m.; C_n^2: 4.4 X 10^{-14}

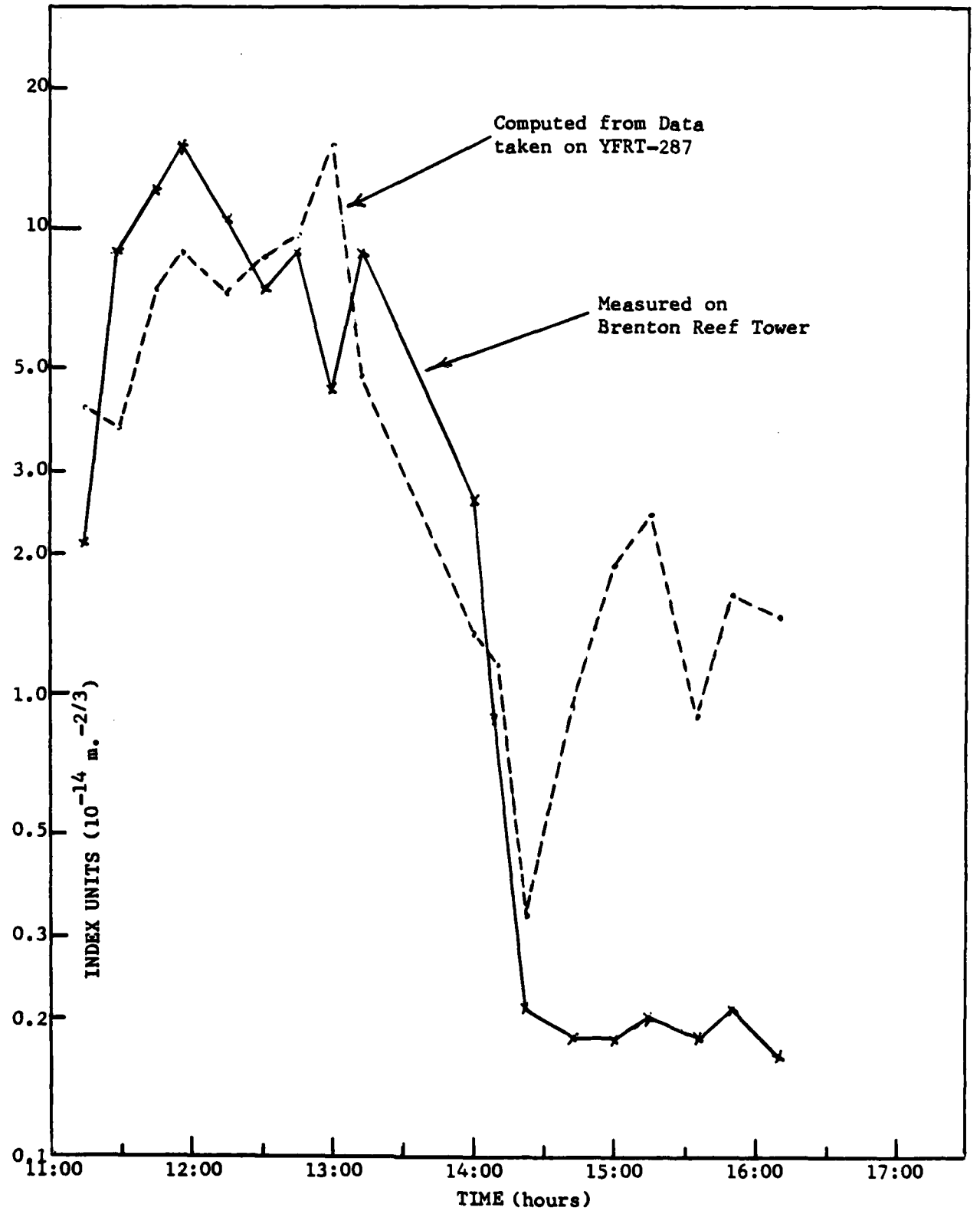

FIGURE 8

COMPARISON OF COMPUTED AND MEASURED VALUES OF C_N^2

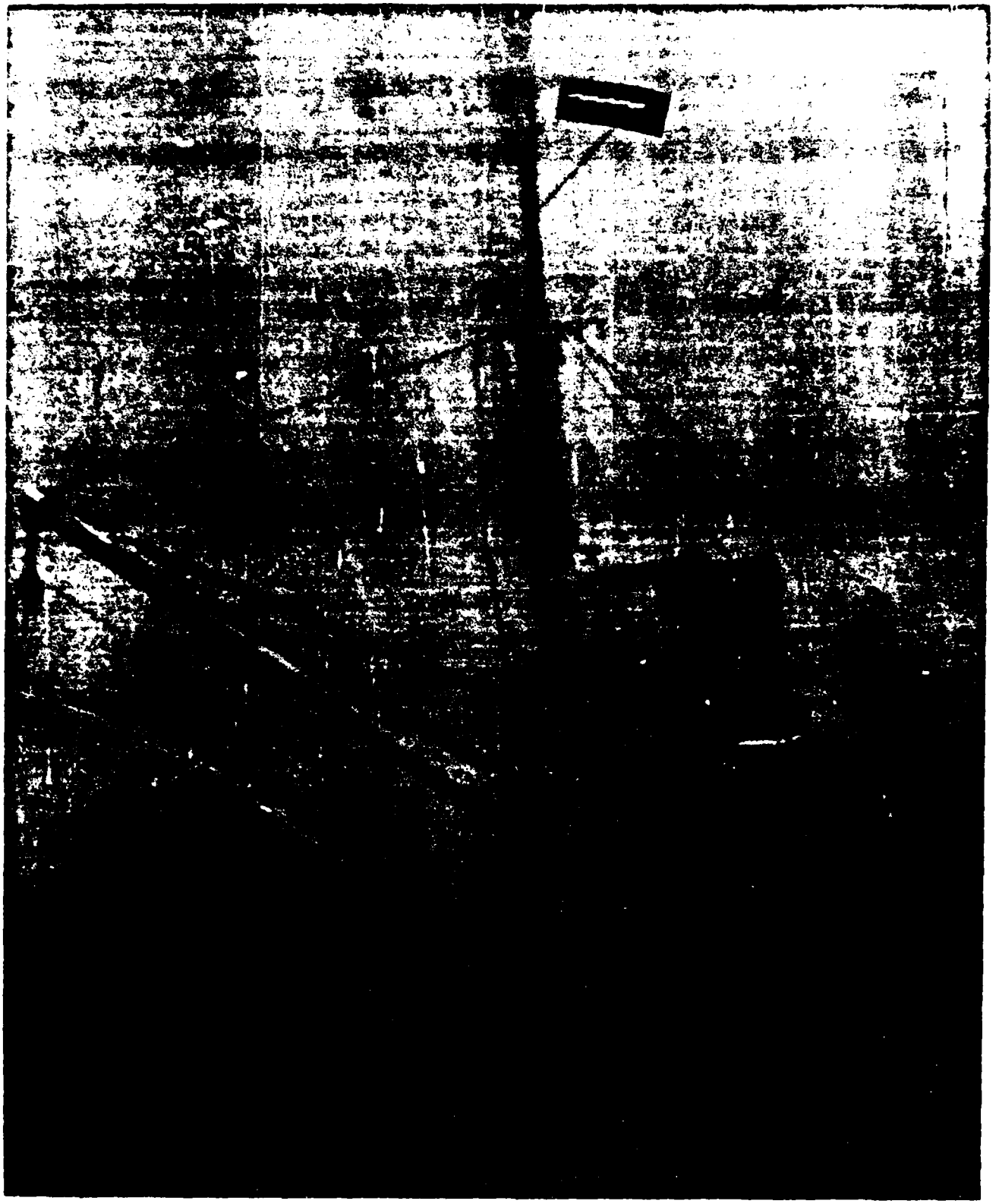

FIGURE 9 ENLARGED PRINT OF IMAGE OBTAINED WITH A WEAKLY TURBULENT ATMOSPHERE
Range: 1000 m.; C_n^2: 2.5×10^{-15}

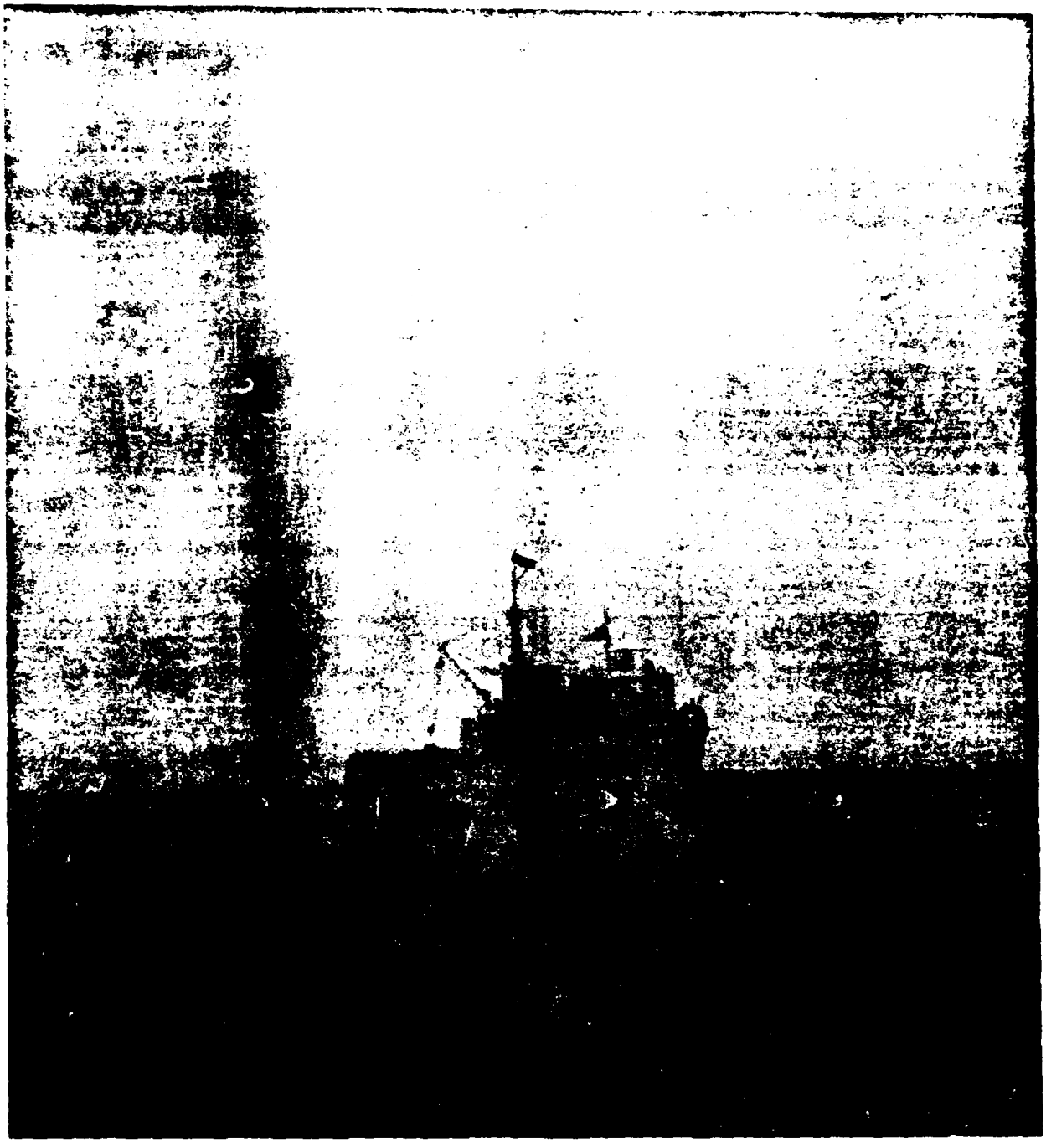

FIGURE 10 ENLARGED PRINT OF IMAGE OBTAINED WITH A WEAKLY TURBULENT ATMOSPHERE
Range: 4970 m.; C_n^2: 0.72 x 10^{-15}

Values of the measured meteorological variables and computed values of C_n^2 for the data taking period of June 6 are shown in Figure 11. The gaps in the curves represent the time interval when the YFRT-287 was transiting to a new anchorage location. The move was necessitated by the earlier shift in the wind direction.

d. 1981 Observation Series

On the expedition of May 8, 1981 a series of about 400 exposures of the target were made, and 77 of these were subsequently scanned by the laboratory's microdensitometer. Each exposure was scanned about three times, and 32 of the exposures were selected as best focussed. From these the line widths representative of the geometrical conditions of the data taking were obtained.

Values of the measured meteorological variables and computed values of C_n^2 are shown in Figure 12. During the time interval from 09:30 to 11:15, values of C_n^2 could not be computed from Equations (5.a and 5.b), since $\xi_0' > 1.25$, and no formulation for the computation of C_n^2 from bulk measurements exists for the highly (buoyantly) stable atmosphere indicated by the measurements.

VI. RESULTS OF OBSERVATIONS

a. General

The three data taking series fall into three categories of atmospheric stability: unstable, neutral, and stable for the 1978, 1980, and 1981 series, respectively. Thus the results are presented separately by years on similar graphs (Figures 13 to 24). Details common to all the graphs follow.

Arrows on the curves indicate the time sequence in which data were taken. Line widths shown represent the distances between points on the film having exposure values with amplitudes 1/e times the peak amplitude. Ordinate scales are linear throughout, except for the "b" series (1978 only) which uses a logarithmic ordinate to illustrate the percentage inaccuracy between computed and measured values of line width. The abscissa of each graph is plotted on a $(\text{range})^{0.6}$ scale, since for a uniformly turbulent path, the image spreading due to turbulence only is proportional to this function of range (c.f. Eq. (24)). Brackets indicate $\pm 1\sigma$ values in the measured widths. The solid line brackets show standard deviation values for the means of all the data. Broken line brackets (1978 only) show standard deviations for a single datum. Adjacent numbers give the number of frames of data used in finding the means and standard deviations. Circles show the mean spread function widths to be expected from computations of C_n^2 and the resulting in optical propagation (c.f. Eq. (24)). The zero range value was obtained by Fourier transforming the combined camera and film responses of (Eq's. (21) and (22)). The ratio of observed to meteorologically predicted line widths for each range (excluding the data for the 500 m range*) have been averaged geometrically for each of the figures. This average ratio is represented on the figures by X.

b. Factors Concerning Specific Data Groups

Table II summarizes factors peculiar to the data groups.

---

* We do this because data from the 1978, 1980, and 1981 observation series show excessive line widths for this near range. We must conclude that factors other than the atmosphere lead to this line broadening.

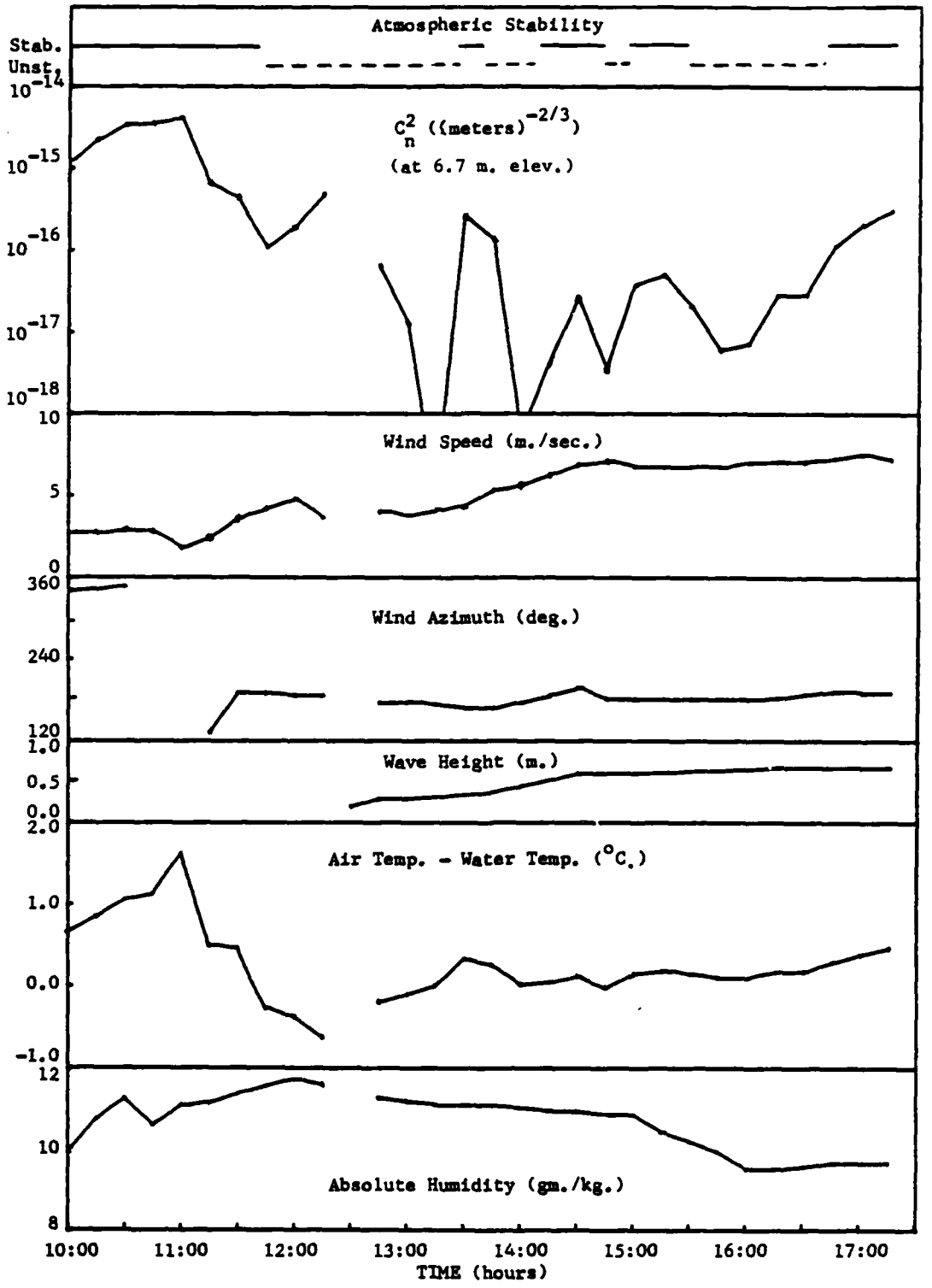

FIGURE 11

VALUES OF METEOROLOGICAL INPUT VARIABLES MEASURED ON THE YFRT-287 AND RESULTING COMPUTED VALUES OF C_n^2---JUNE 6, 1980

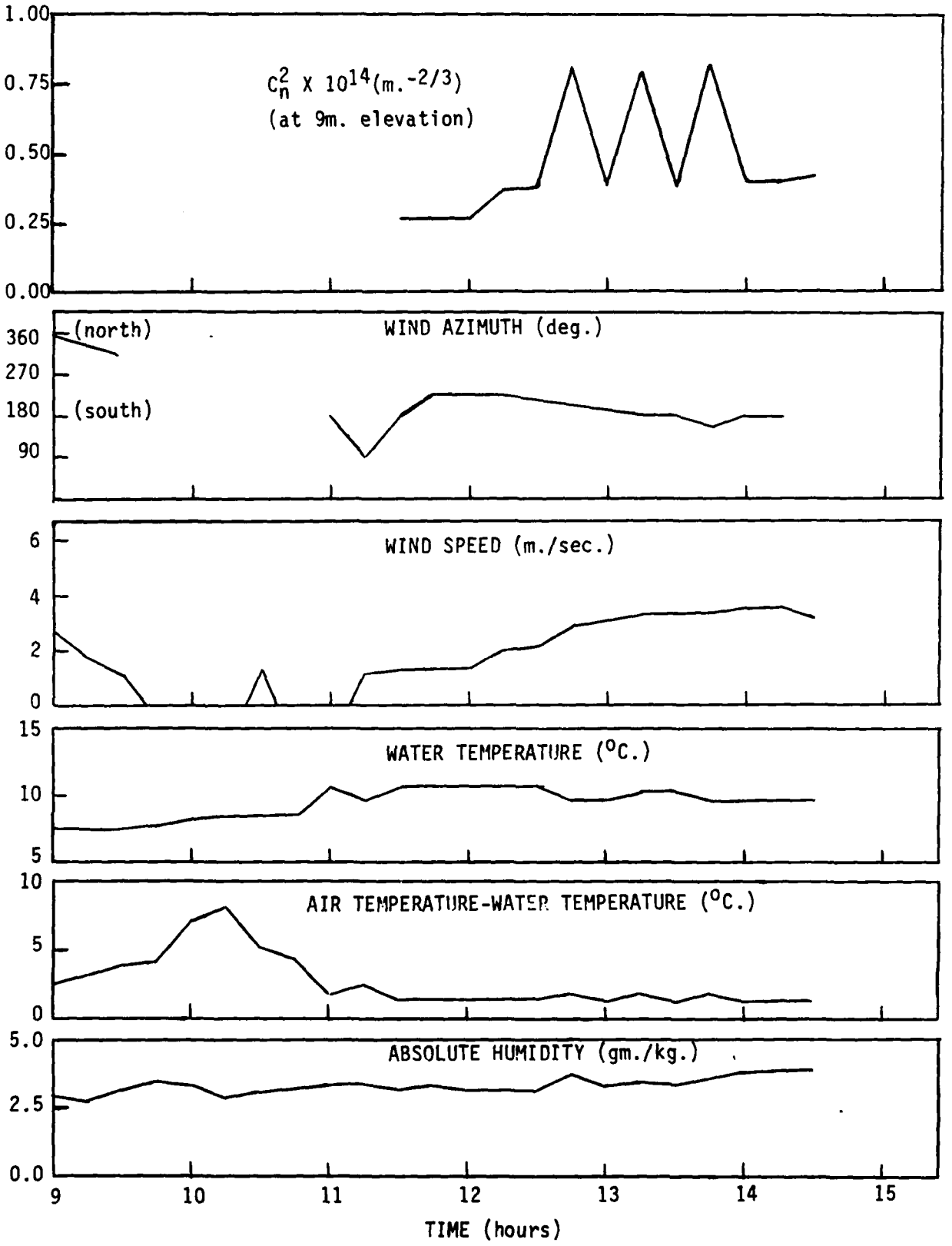

FIGURE 12

METEOROLOGICAL DATA TAKEN ON MAY 8, 1981
AND RESULTING COMPUTED VALUES OF C_n^2

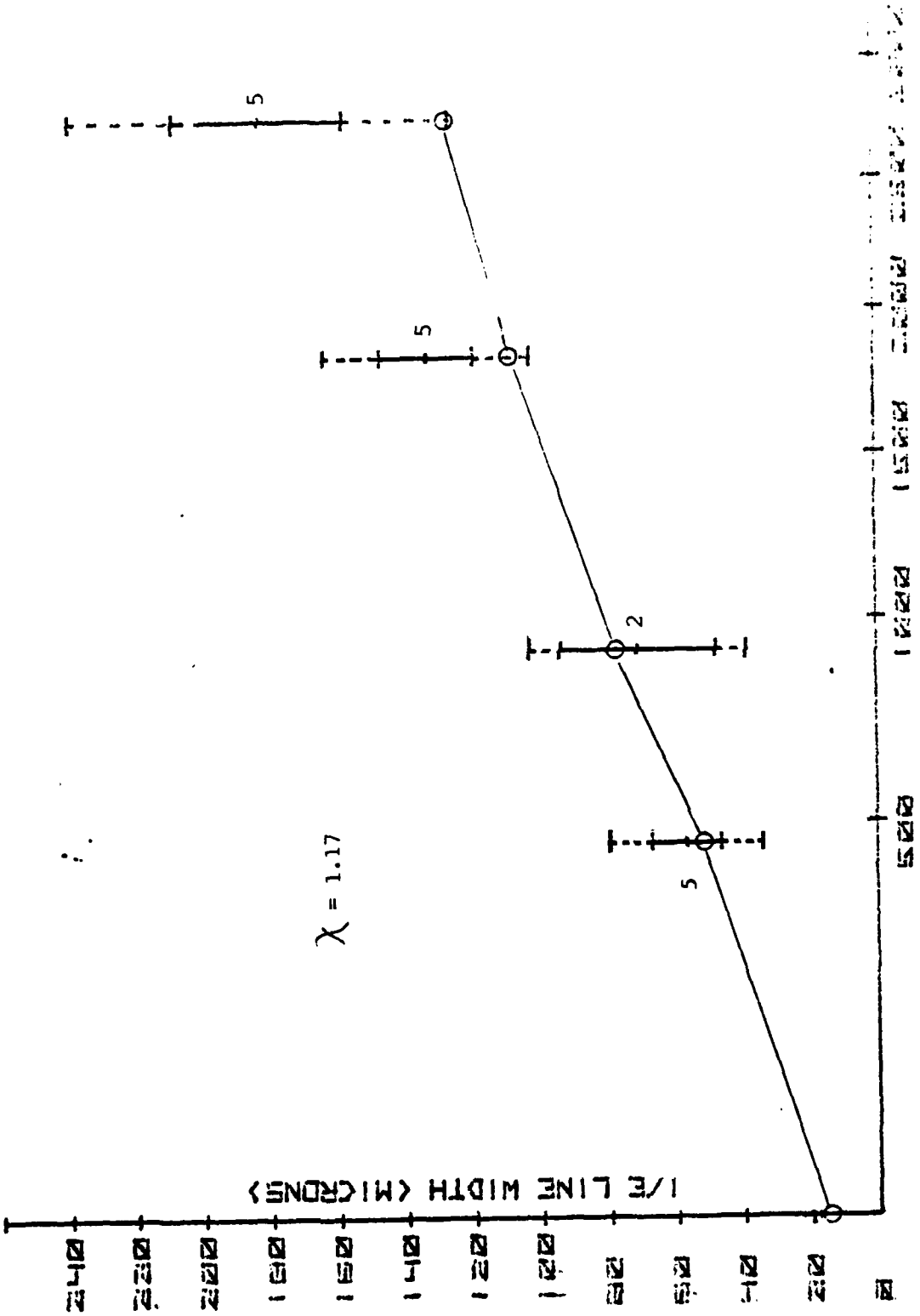

Figure 13.a THEORETICAL (CIRCLES) AND MEASURED LINE WIDTHS FOR OBSERVATION SERIES A AS A FUNCTION OF TARGET RANGE

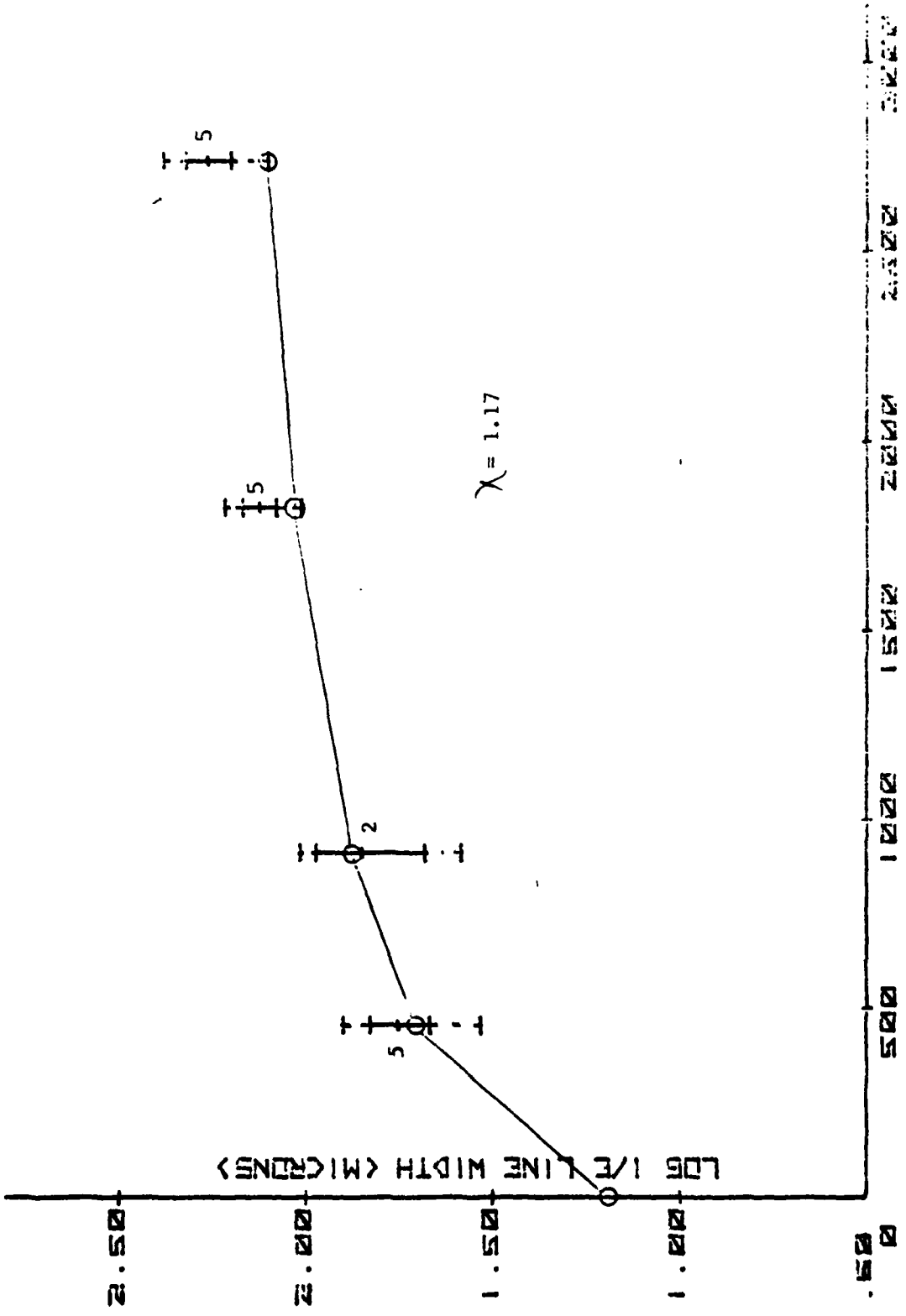

Figure 13.b THEORETICAL (CIRCLES) AND MEASURED LINE WIDTHS FOR OBSERVATION SERIES A AS A FUNCTION OF TARGET RANGE

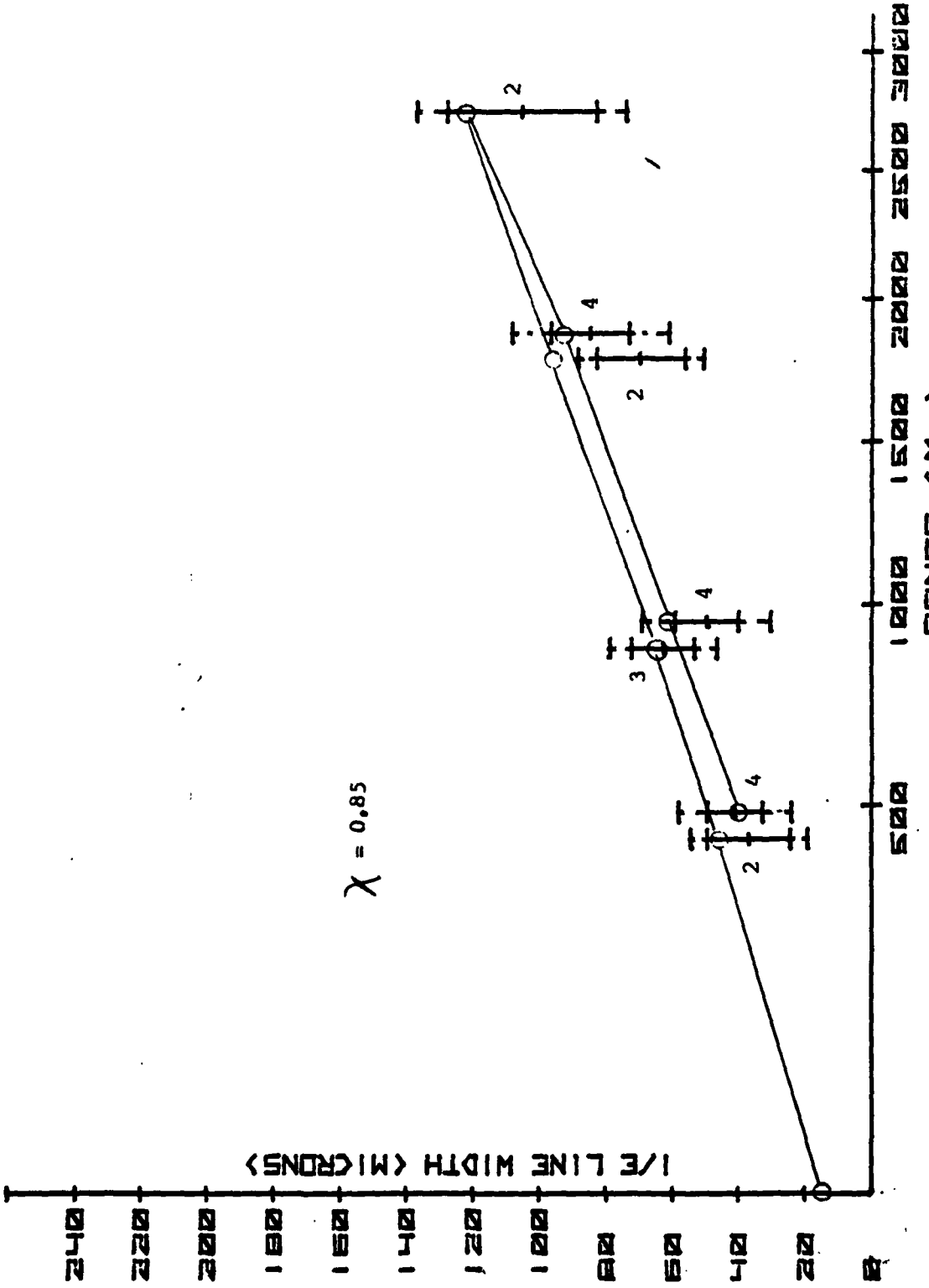

Figure 14.a THEORETICAL (CIRCLES) AND MEASURED LINE WIDTHS FOR OBSERVATION SERIES B AS A FUNCTION OF TARGET RANGE

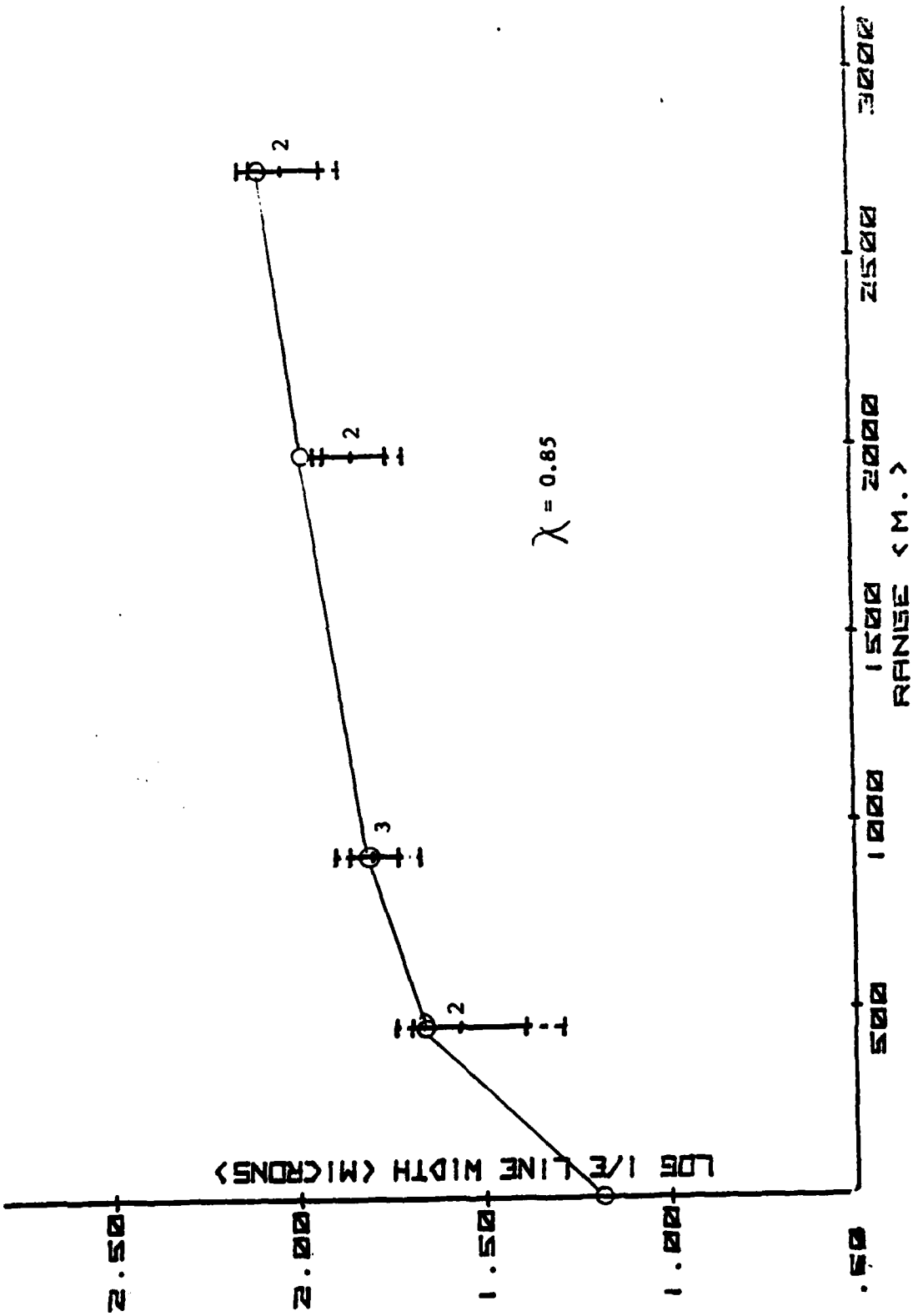

Figure 14.b THEORETICAL (CIRCLES) AND MEASURED LINE WIDTHS FOR OBSERVATION SERIES B AS A FUNCTION OF TARGET RANGE

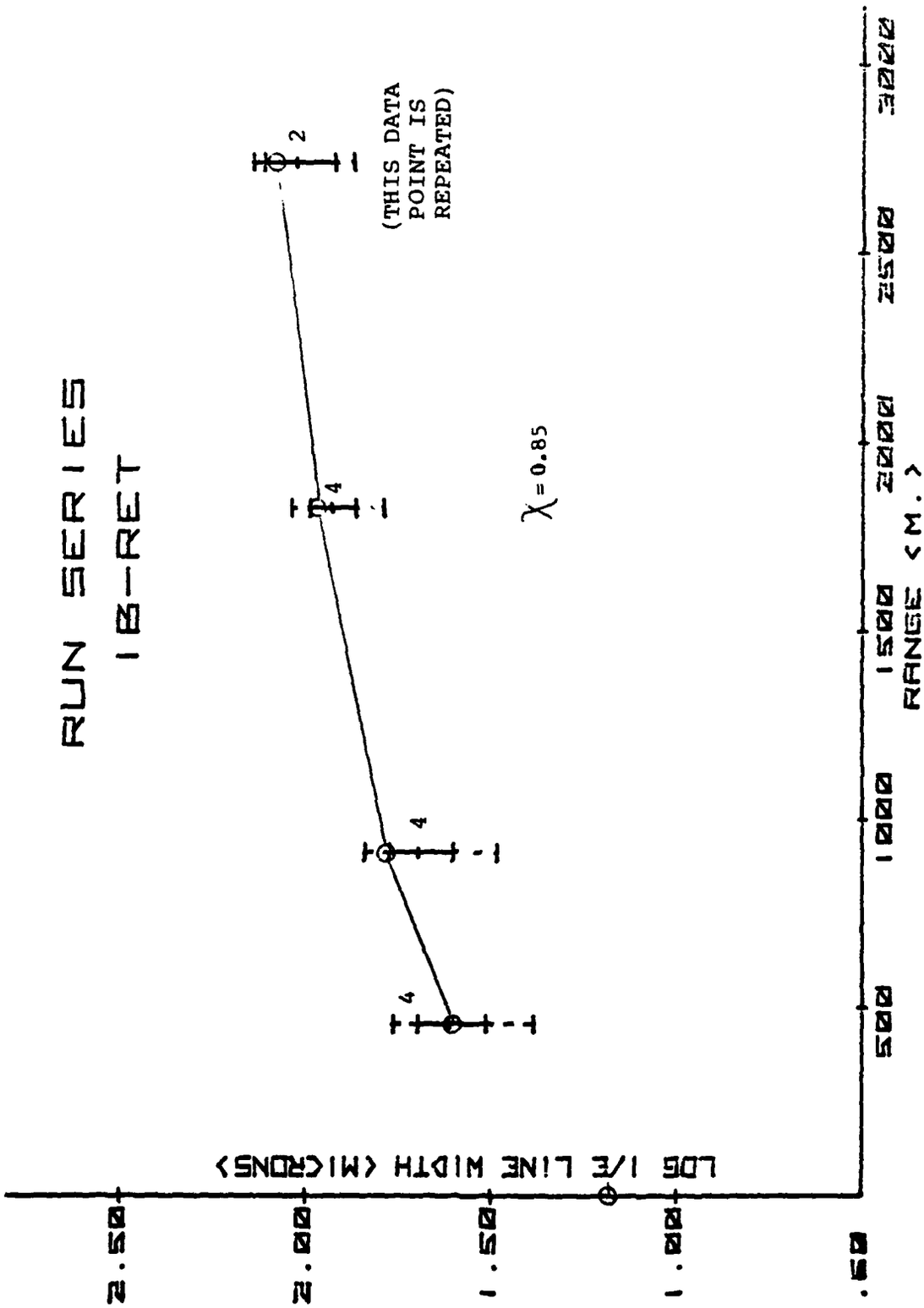

Figure 14.c THEORETICAL (CIRCLES) AND MEASURED LINE WIDTHS FOR OBSERVATION SERIES B (CONT'D) AS A FUNCTION OF TARGET RANGE

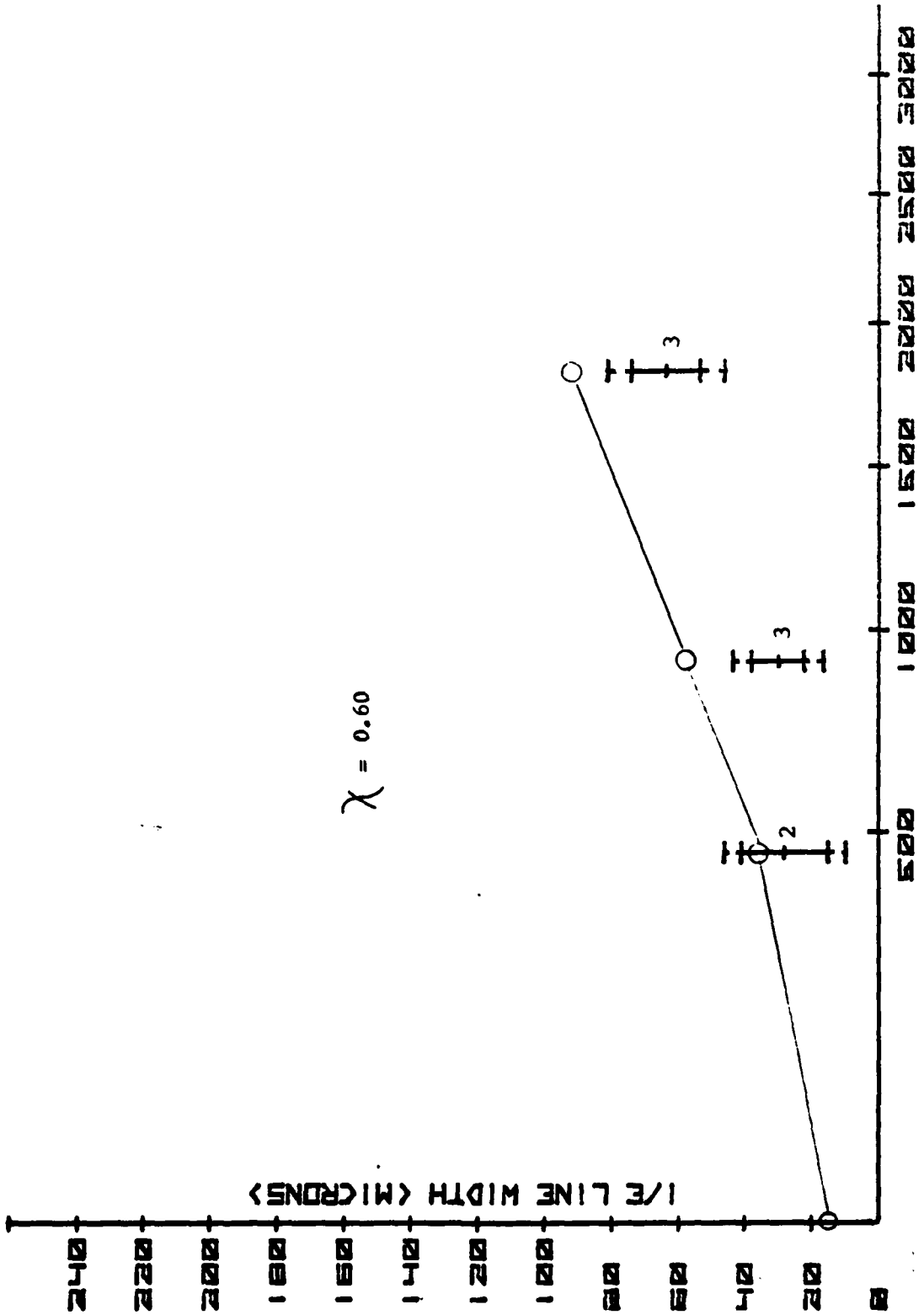

Figure 15.a THEORETICAL (CIRCLES) AND MEASURED LINE WIDTHS FOR OBSERVATION SERIES C AS A FUNCTION OF TARGET RANGE

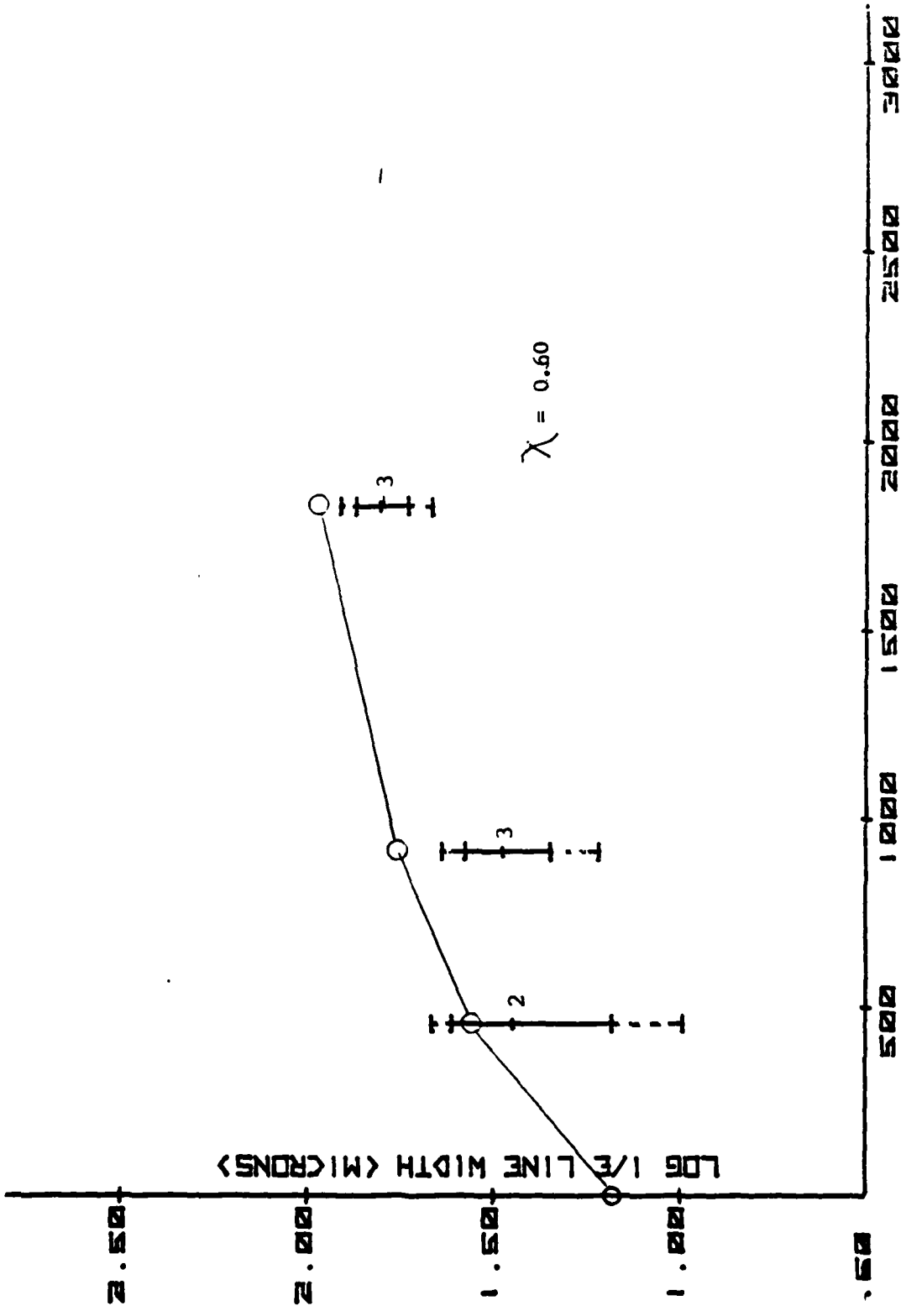

Figure 15.b THEORETICAL (CIRCLES) AND MEASURED LINE WIDTHS FOR OBSERVATION SERIES C AS A FUNCTION OF TARGET RANGE.

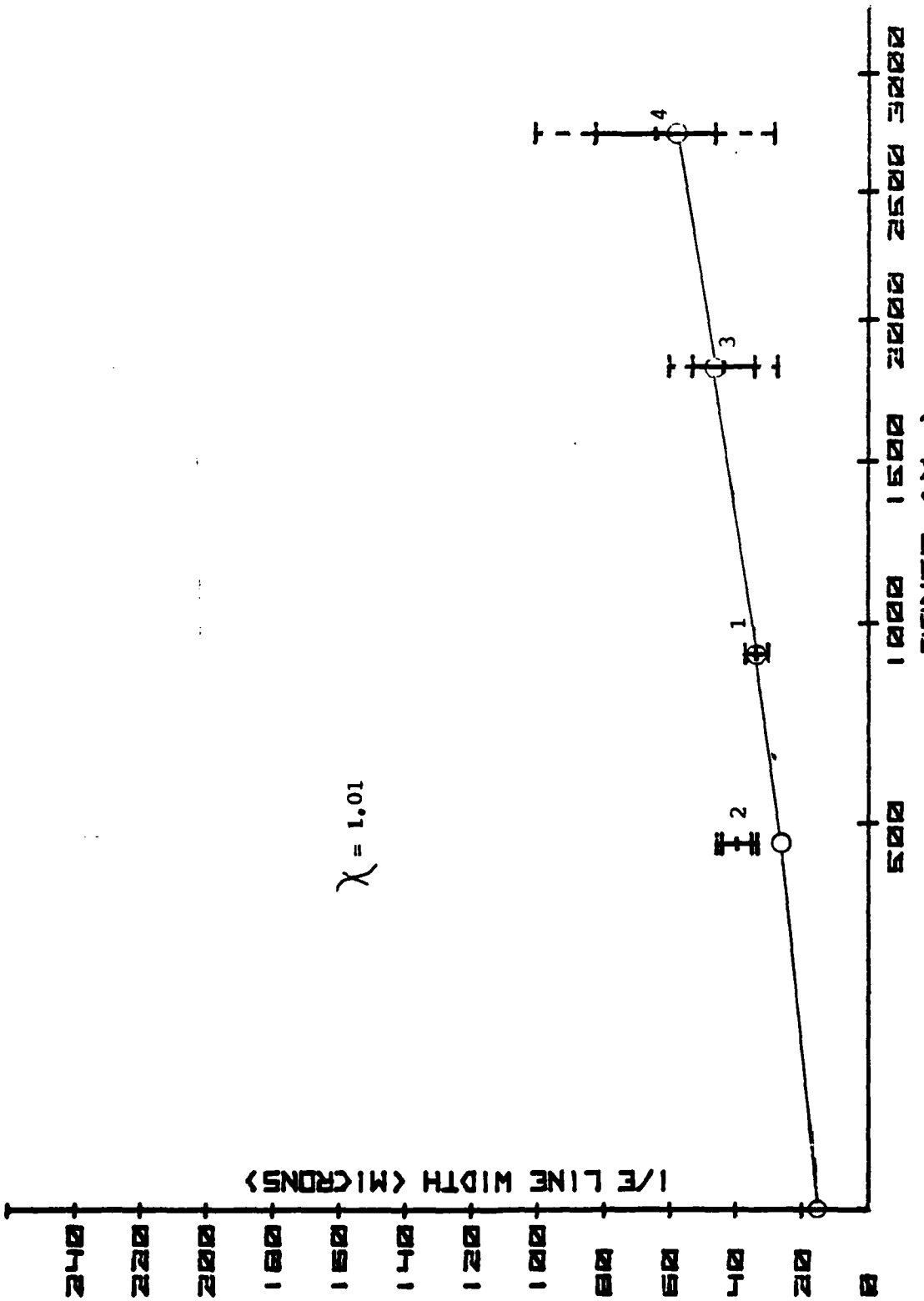

Figure 16.a THEORETICAL (CIRCLES) AND MEASURED LINE WIDTHS FOR OBSERVATION SERIES F AS A FUNCTION OF TARGET RANGE

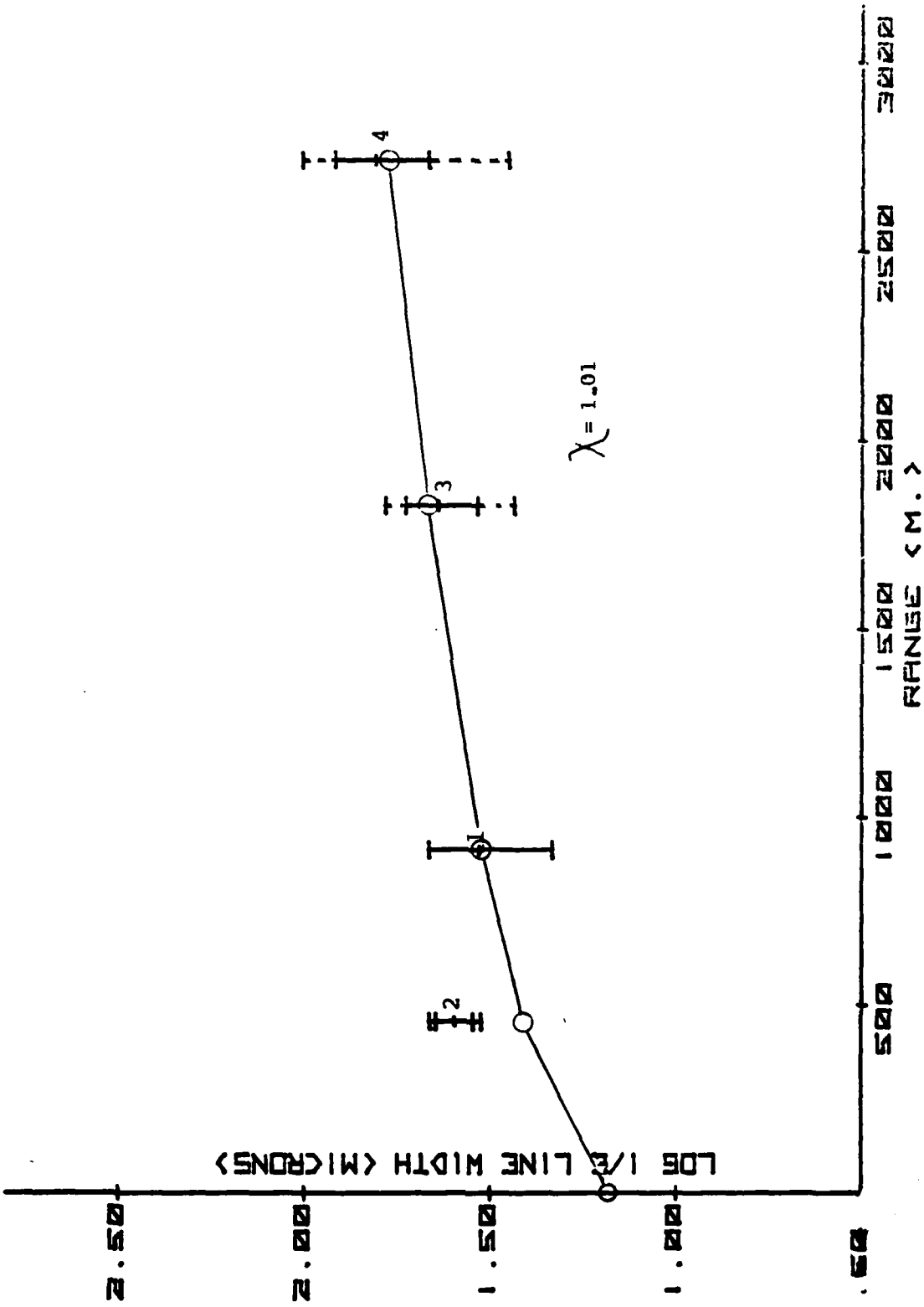

Figure 16.b THEORETICAL (CIRCLES) AND MEASURED LINE WIDTHS FOR OBSERVATION SERIES F AS A FUNCTION OF TARGET RANGE

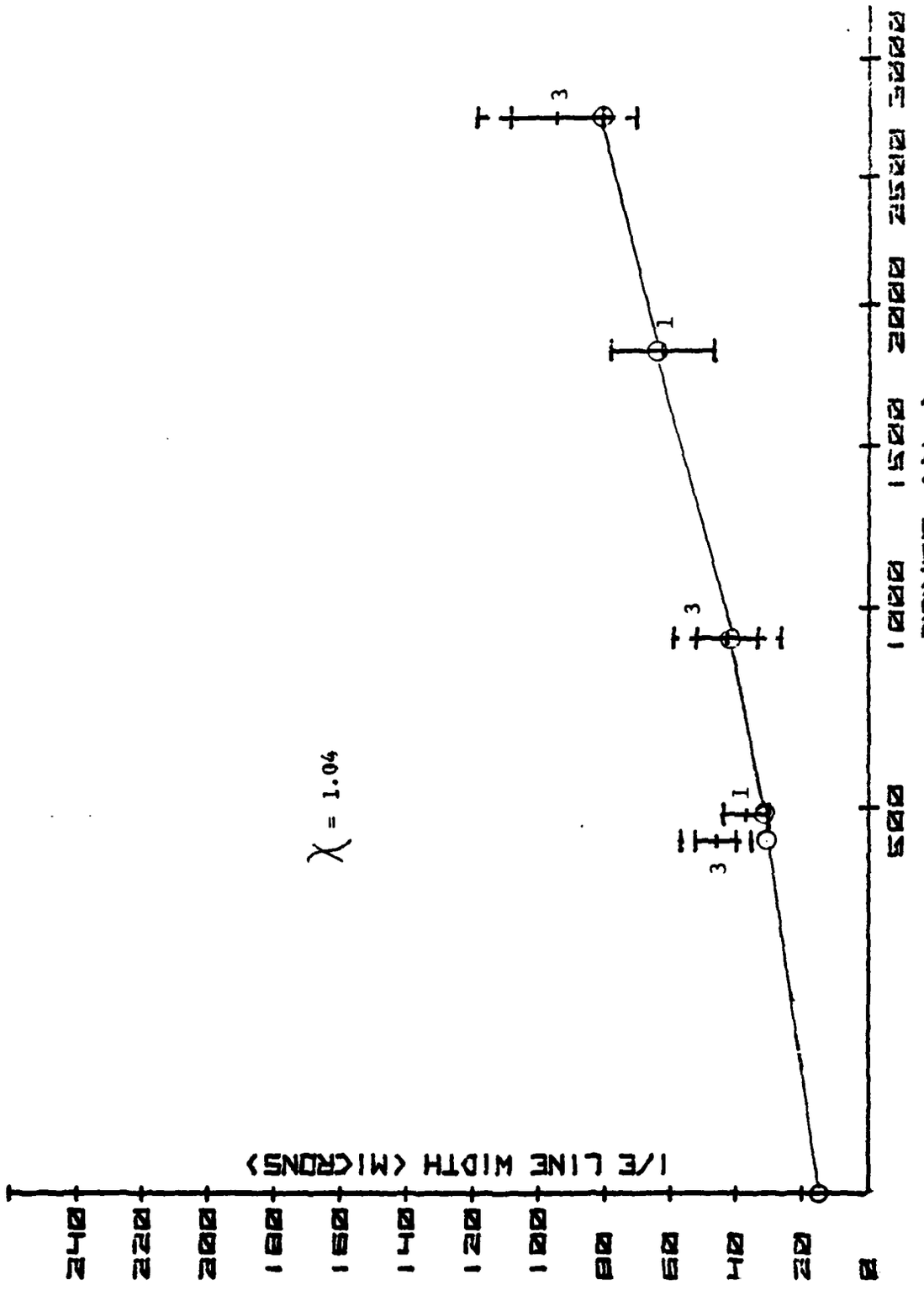

Figure 17.a THEORETICAL (CIRCLES) AND MEASURED LINE WIDTHS FOR OBSERVATION SERIES G AS A FUNCTION OF TARGET RANGE

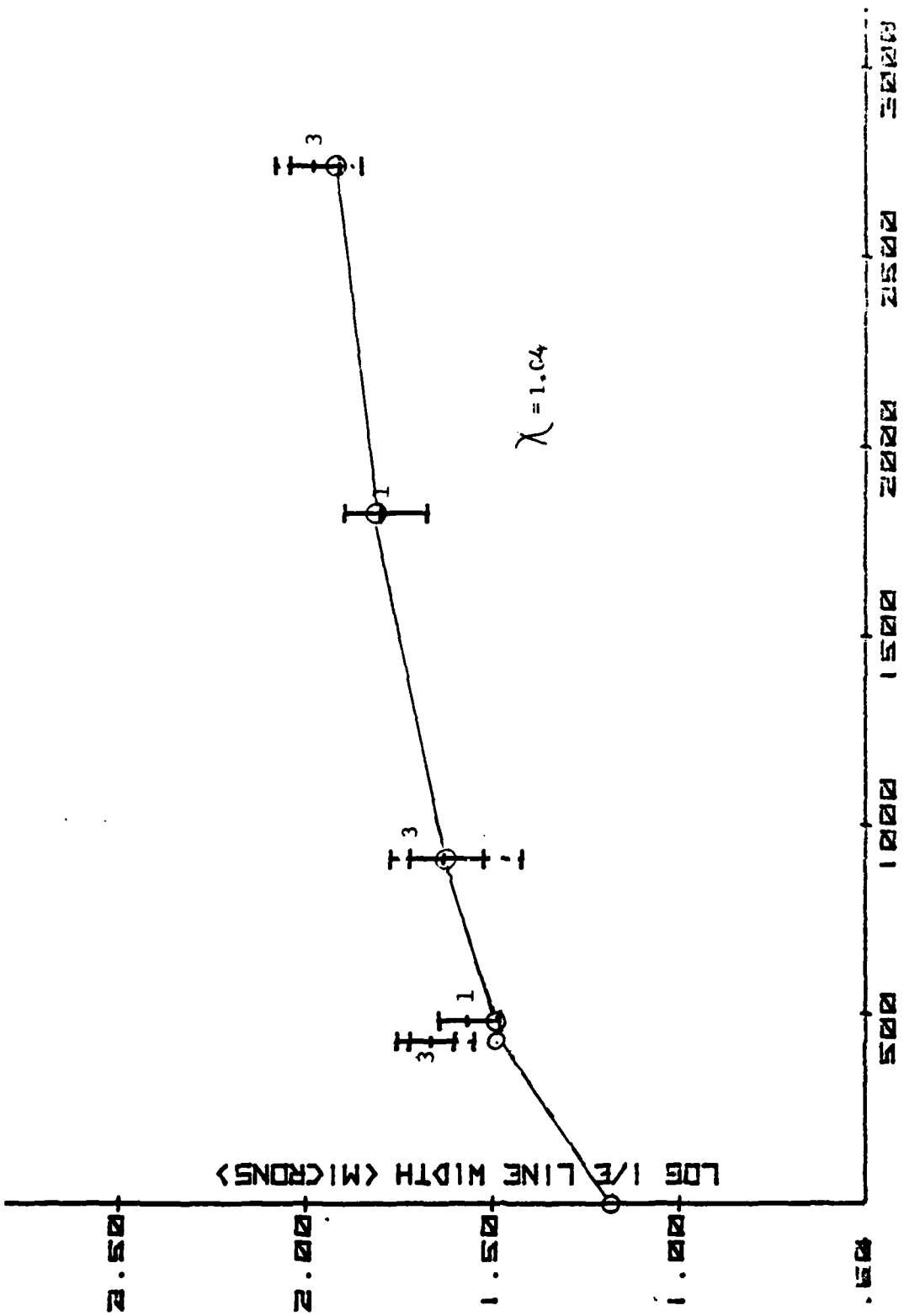

Figure 17.b THEORETICAL (CIRCLES) AND MEASURED LINE WIDTHS FOR OBSERVATION SERIES G AS A FUNCTION OF TARGET RANGE

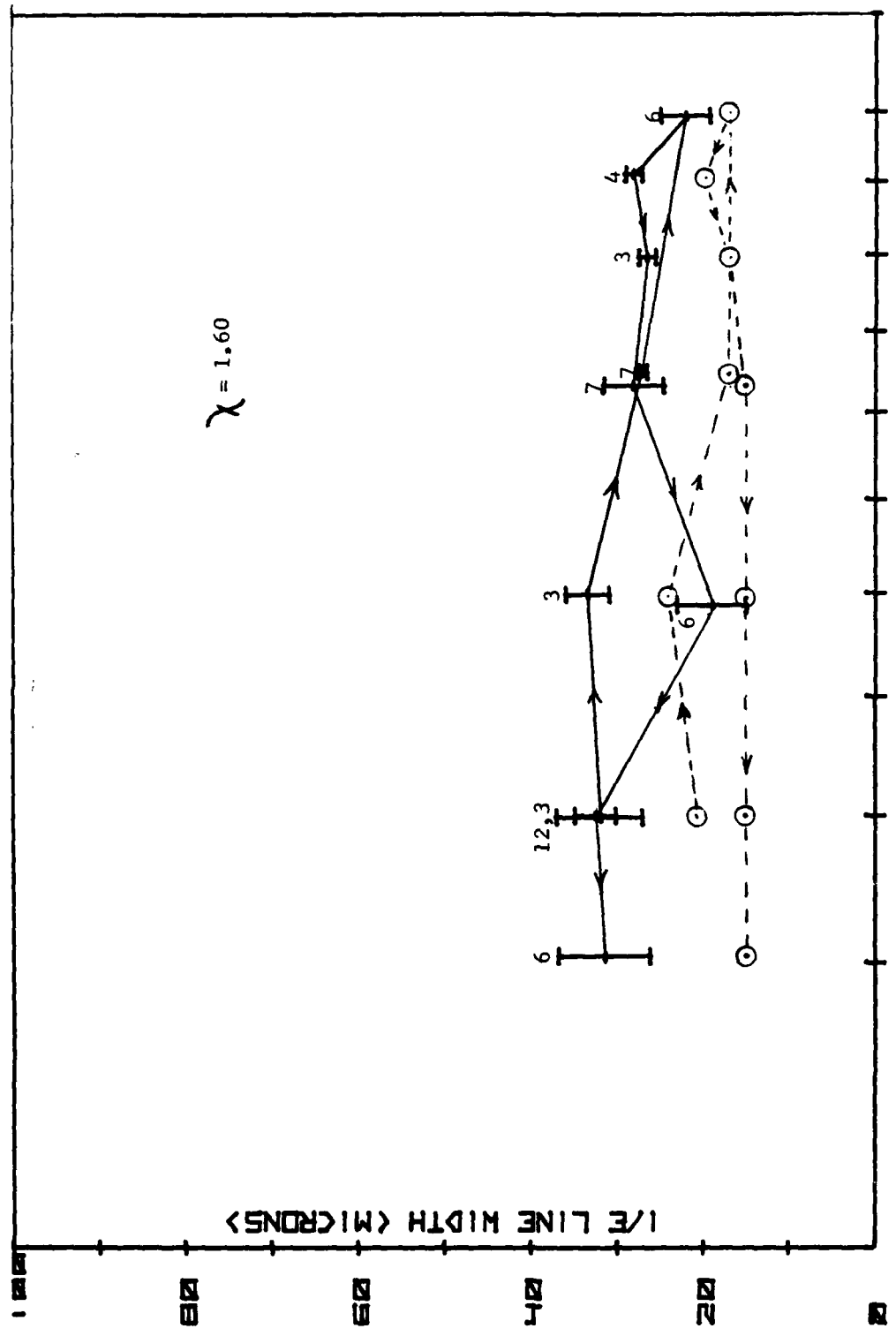

FIGURE 18
THEORETICAL (CIRCLES) AND MEASURED LINE WIDTHS FOR OBSERVATION SERIES H AS A FUNCTION OF TARGET RANGE

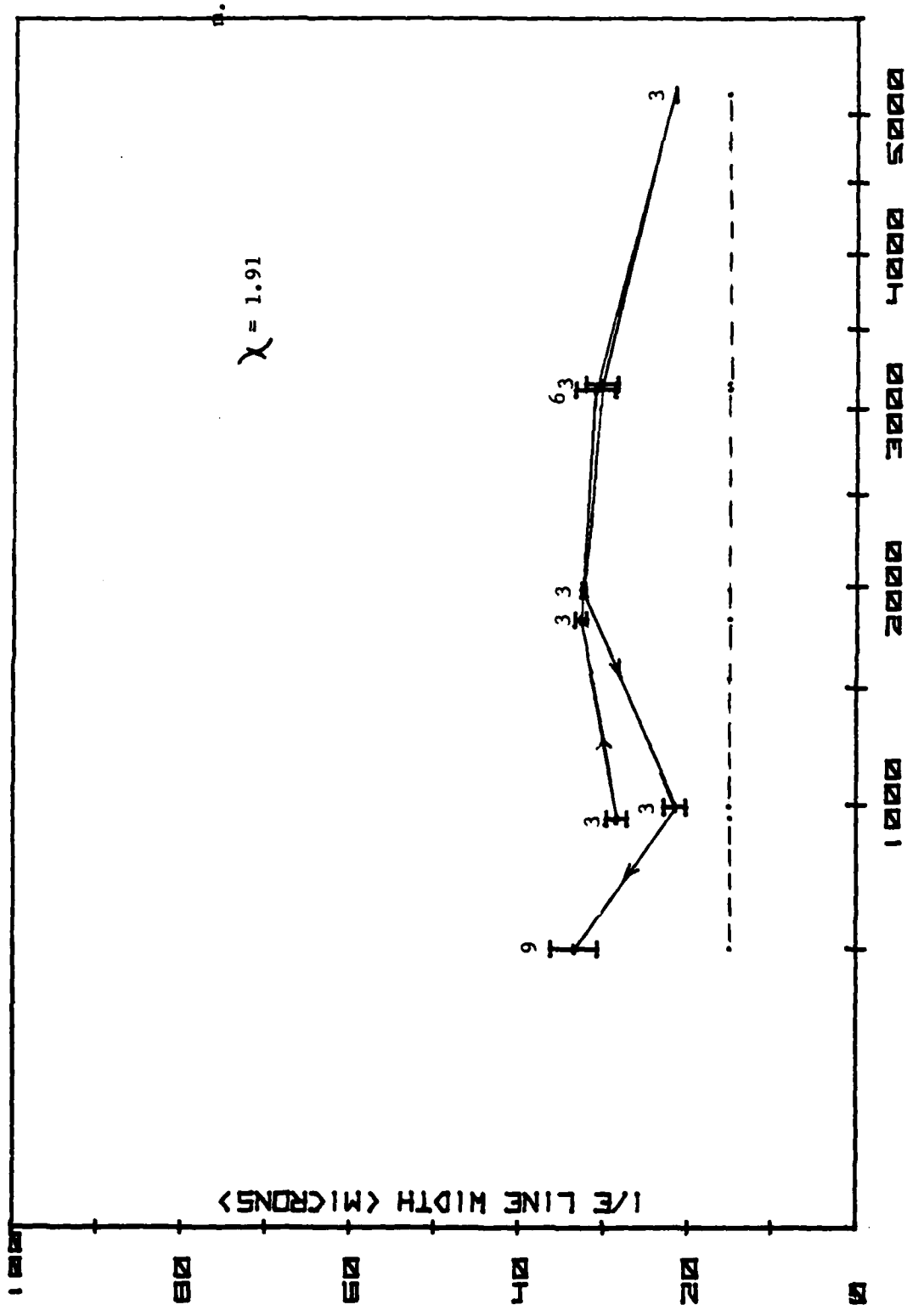

FIGURE 19

THEORETICAL (CIRCLES) AND MEASURED LINE WIDTHS FOR OBSERVATION SERIES I AS A FUNCTION OF TARGET RANGE

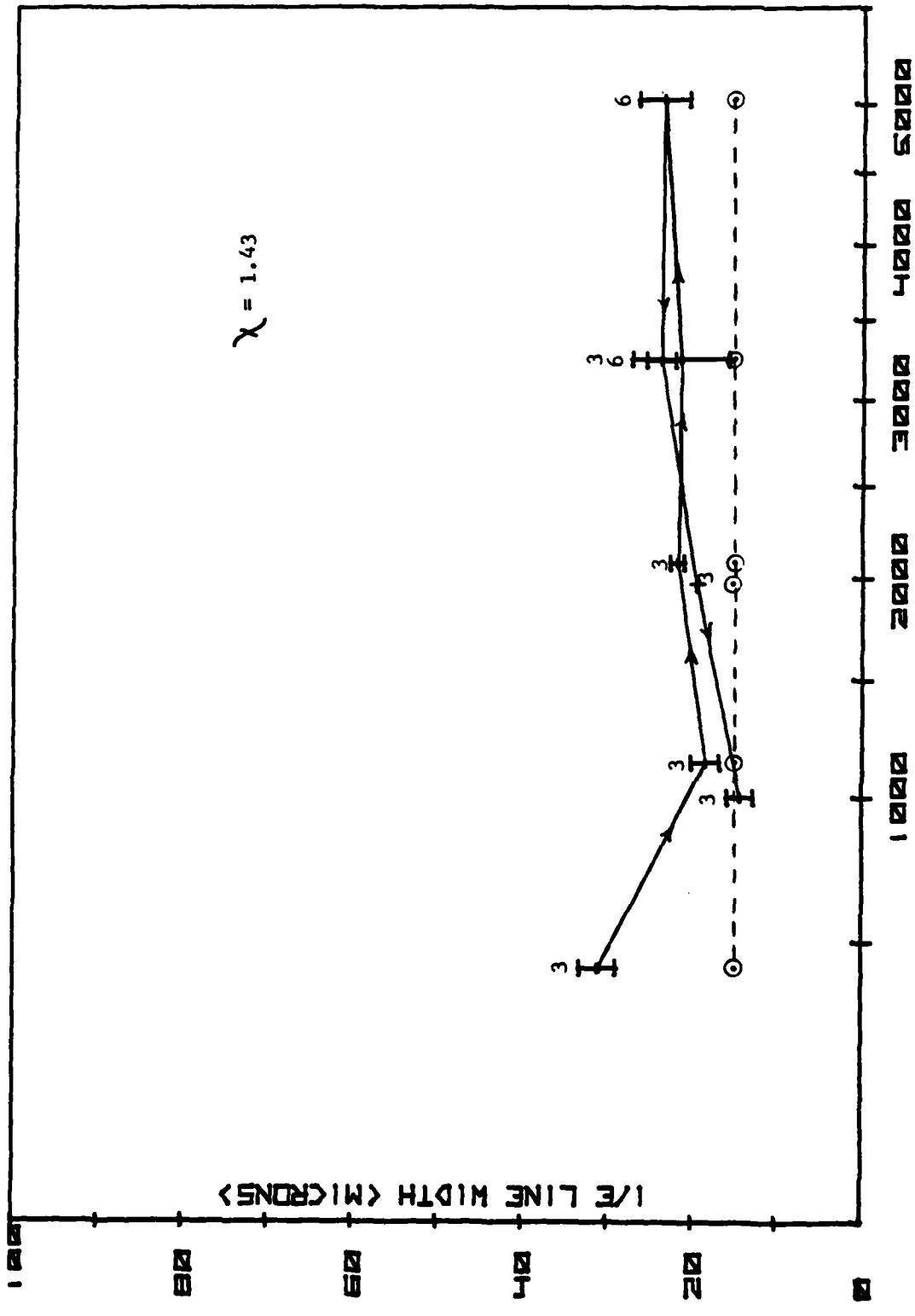

FIGURE 20
THEORETICAL (CIRCLES) AND MEASURED LINE WIDTHS FOR OBSERVATION SERIES J AS A FUNCTION OF TARGET RANGE

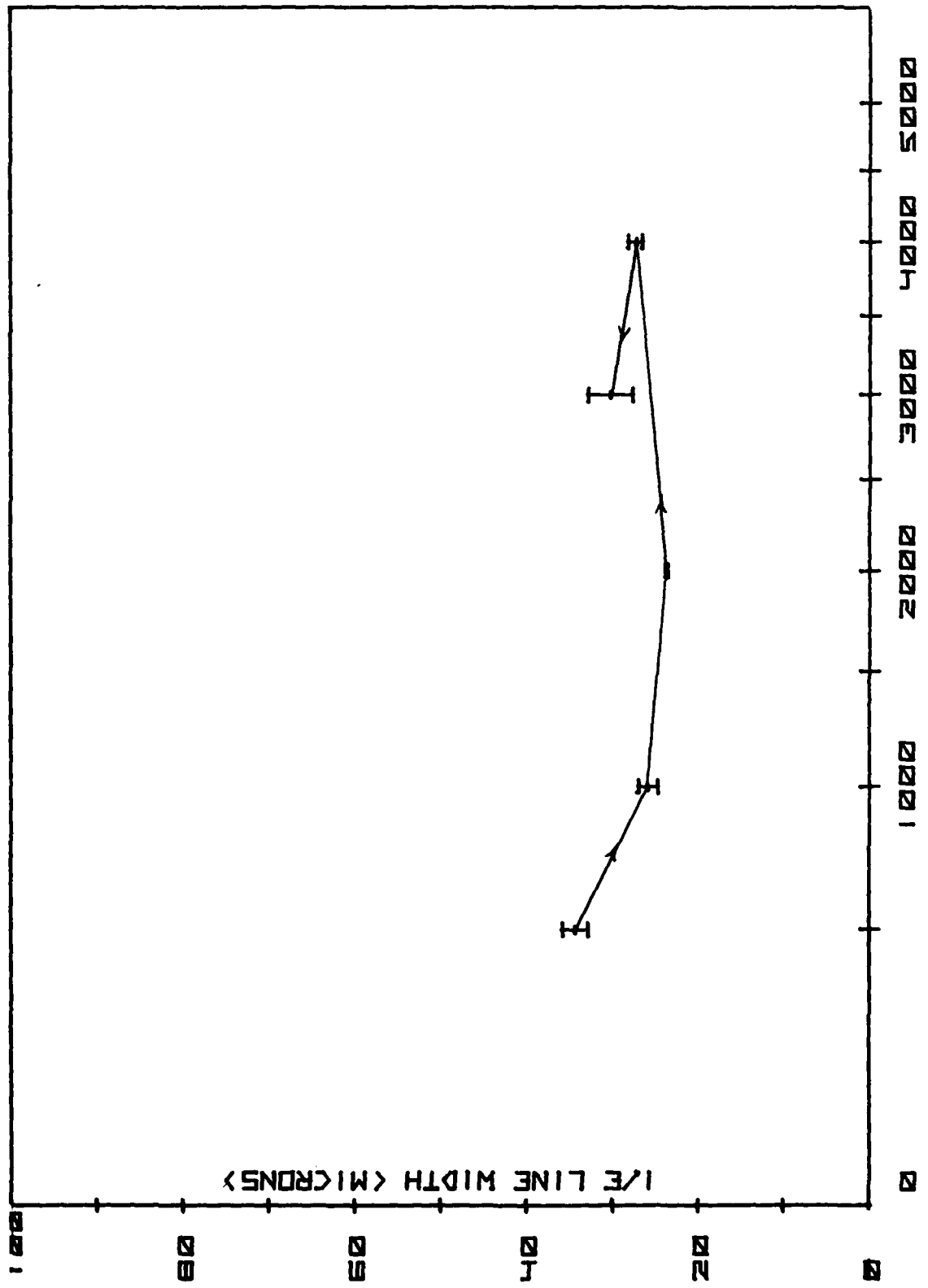

FIGURE 21

MEASURED LINE WIDTHS FOR OBSERVATION
SERIES K AS A FUNCTION OF TARGET RANGE

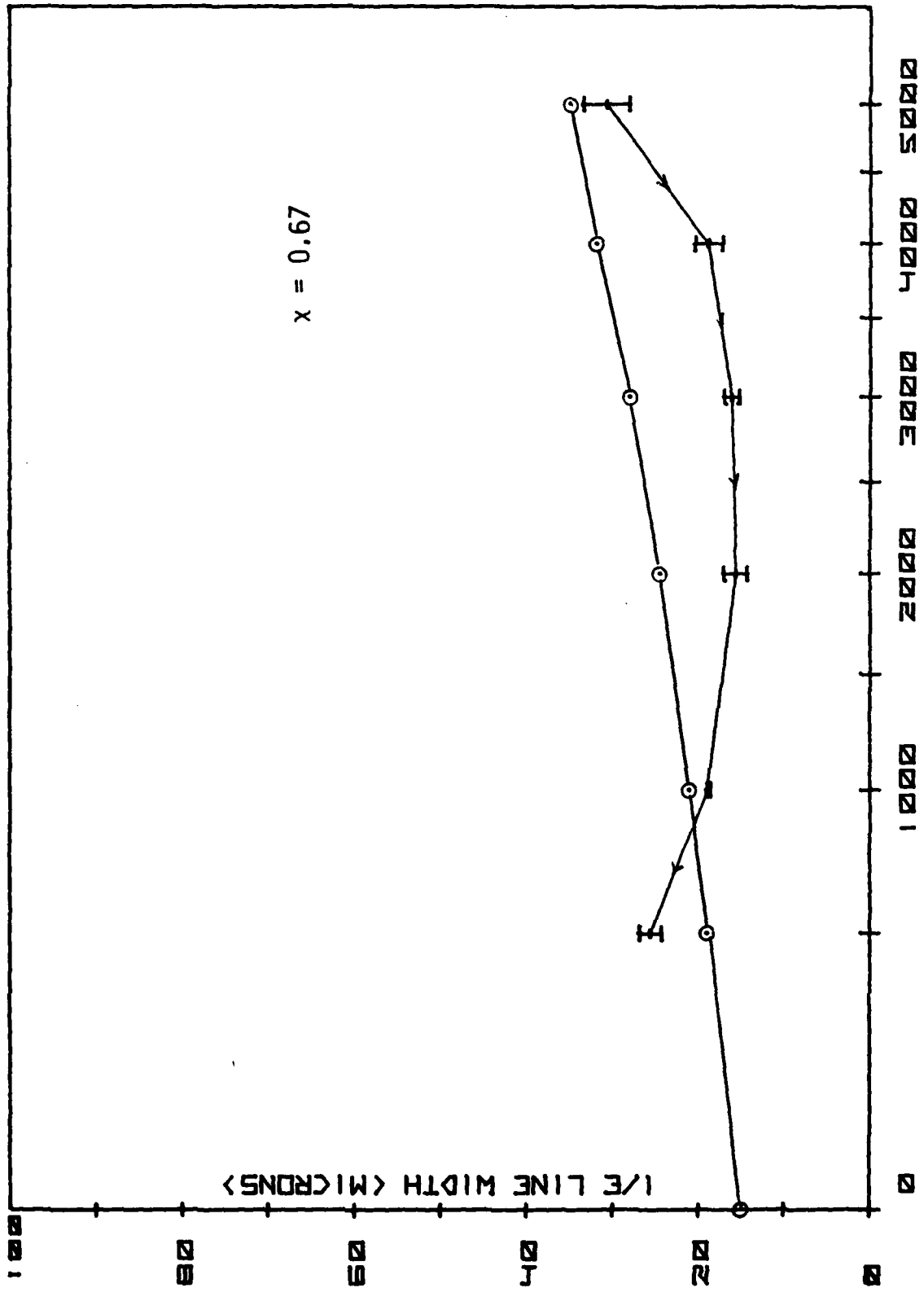

FIGURE 22
THEORETICAL (CIRCLES) AND MEASURED LINE WIDTHS FOR OBSERVATION SERIES L AS A FUNCTION OF TARGET RANGE

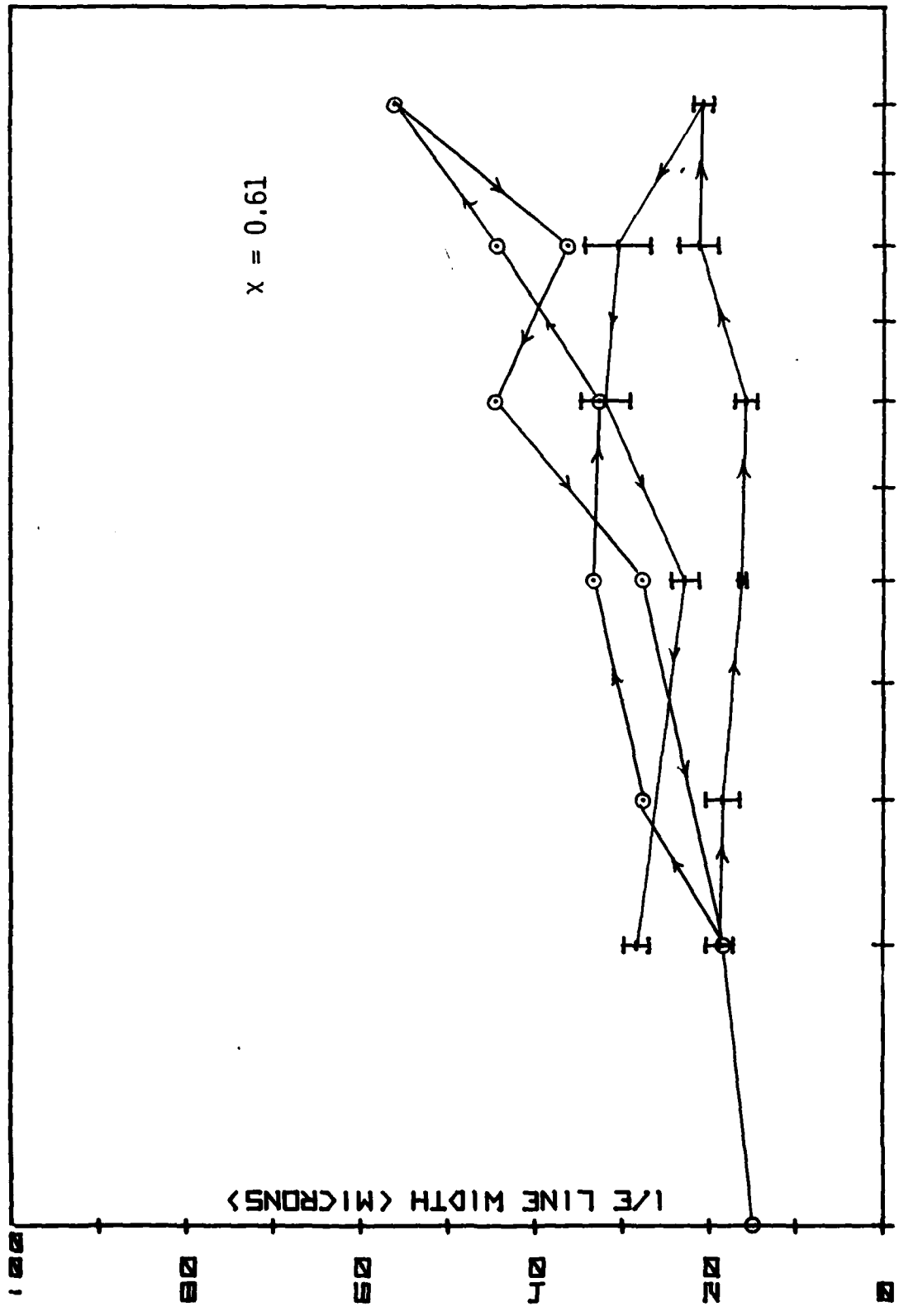

FIGURE 23
THEORETICAL (CIRCLES) AND MEASURED LINE WIDTHS FOR OBSERBATION SERIES M AS A FUNCTION OF TARGET RANGE

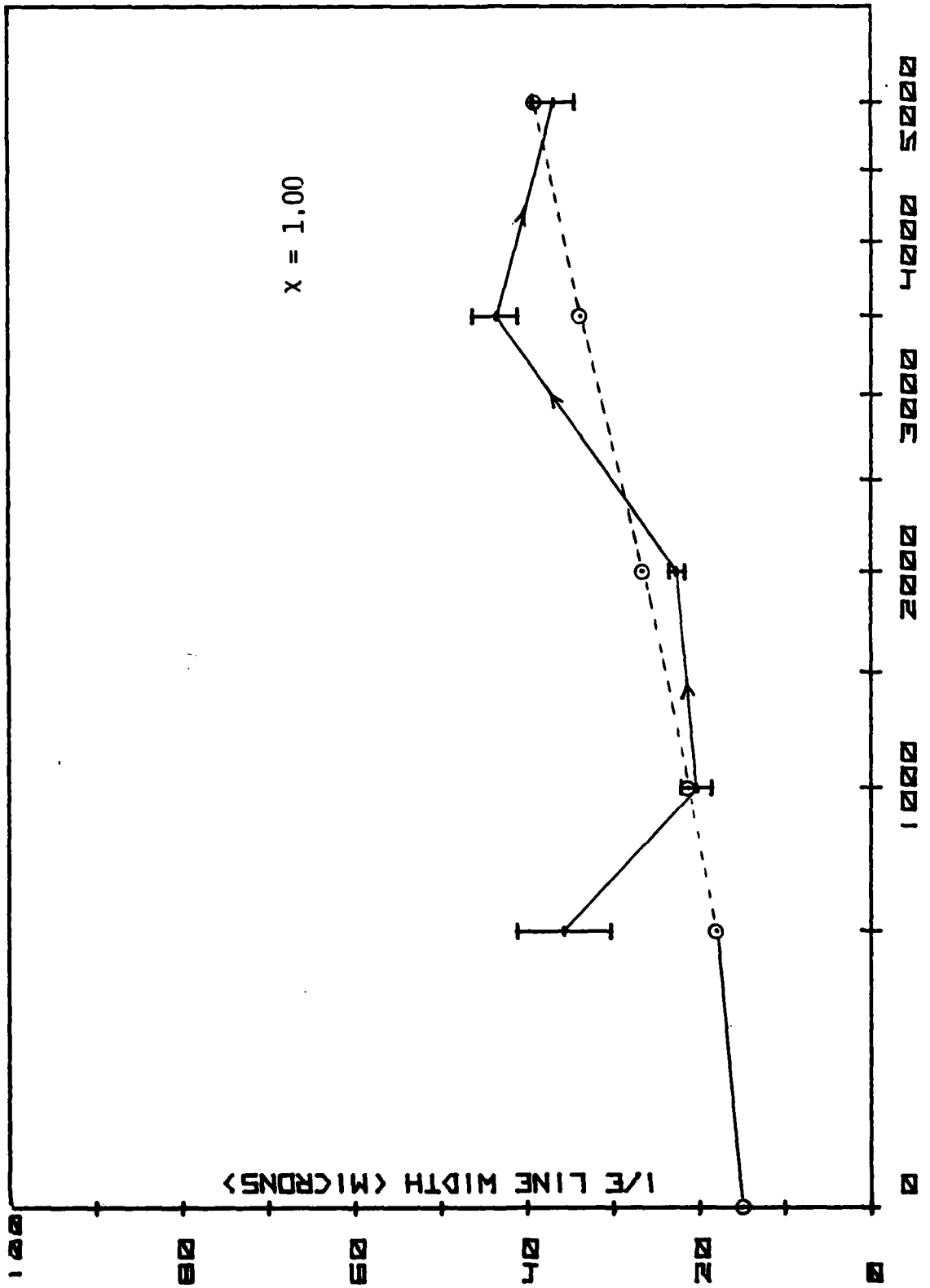

FIGURE 24
THEORETICAL (CIRCLES) AND MEASURED LINE WIDTHS FOR OBSERVATION SERIES N AS A FUNCTION OF TARGET RANGE

Table II. Factors Specific to Data Groups

Date	Time Interval	Figure No's	Turbulence Strength	Atmospheric Stability	Geometric Mean of X Values	Notes
9/26/78	10:00-15:00	16.a-18.b	Very Strong	Unstable	0.84	
9/27/78	12:30-14:00	19.a-20.b	Strong	Unstable	1.11	
6/6/80	10:55-17:15	21-23	Very Weak	Variable	1.63	The atmosphere was essentially neutral during this time interval.
5/8/81	10:05-15:00	24-27	Light	Stable	0.74	Computed line width values are omitted from Figure 24 since meteorological parameter readings fell outside of the range of possible computation. All computed line width values on Figure 27 were obtained from meteorological observations made at 14:30.

VII. DISCUSSION OF RESULTS

a. Unstable Atmosphere with Strong Turbulence

Under these conditions we note that mean values of measured line widths differ at most by a factor of two from values predictable from bulk meteorological measurements. This is in approximate agreement with the factor of two accuracy which Davidson, et alia,[4] obtained the index structure constant from bulk meteorological measurements.* It is significant that the geometric mean of the ratio of observed to predicted line widths for the full set of data is much closer than this, viz., 0.91/1, indicating that when space and time variations are averaged out, the correspondence of theory with mean turbulence conditions is much closer. A careful look at the detailed records of ambient conditions (Figures 6 present 30 minute averages) shows that from 12:00 to 15:00 on September 26, the wind speed was highly variable. values for data series B and C (Figures 15 and 16) for the intervals 11:45-12:50 and 14:00-14:30 on this day are 0.85 and 0.60: giving a geometric mean of 0.71; whereas the values for the other data series, A, F and G, are 1.17, 1.01, and 1.04, giving a geometric mean of 1.07.

Concerning single line width observations--an aspect which has not been treated theoretically--we note that the 1σ fractional deviation from the mean value, averaged over the set of ranges (excluding 460 m.) and times was 34 percent of the mean. The maximum 1σ value at maximum range was 86 percent.

b. Neutral Atmosphere

In this series of observations the measured line width values are higher than the calculated values and essentially independent of target range. This points to an instrumental limitation in the achievable line width, apparently about 25 to 30 microns.

In Figure 18, a correlation of measured line width with computed line width is shown at ranges of 2990 and 4550 m. At these times, the products of C_n^2 (computed for a height of 6.67 m.) and ranges were 8.0 and 2.1 x 10^{-14} $m.^{1/3}$. From this data one concludes that if an ideal camera located one meter above the sea surface records images of a ship or shore in a millisecond exposure, the images will have a mean line spread of 2.5 arc seconds** or less if the two primary ambient conditions are met:

1. Air Temperature - Water Temperature $\leq$ 1.25°C (stable atmosphere).
2. Wind Speed $\geq$ 2.0 m./sec. = 3.9 knots.

---

* A factor of two agreement in line width can be shown to be equivalent to a factor of three agreement in the values of C_n^2 .

** This value is obtained by rss subtraction of the limiting value of the line width produced by the equipment from the mean measured line width values. It also corresponds approximately with the line width predicted for an ideal camera with a C_n^2 x range product of 8.0 x 10^{-14} $m.^{1/3}$ with a stable atmosphere.

As a spot check on the range dependence of the mean line widths, we noted that in Figures 16b and 17b, where the temperature and wind conditions were stabilized, the (range)$^{0.6}$ dependence of the line width was followed with a deviation of less than 6 percent over the range span 920 to 2740 m. As a spot check on the camera elevation factor, we compared two measured line width values at a range of 2740 m. With C_n^2 values nearly the same, lowering the camera from a height of 2.3 m. (Figure 16) to 0.8 m. (Figure 17) increased the line width by 47 percent; whereas theoretically this change (allowing for different L values) should produce a change of only 40 percent. The difference ratio, 1.47/1.40 = 1.05, is so close to 1.0 that we conclude that the camera height formulation is correct.

Because of the indicated correspondences between measured mean and theoretical values of line spread, we conclude that the theoretical formulations are accurate within tens of percent for these turbulence conditions for target ranges from 910 to 2740 m. and wind speeds from 2 to 7 m./sec. and camera elevations from the surface of the ocean from 0.8 to 2.4 m.

c. Stable Atmosphere -- Weak Turbulence

Since the particularly high air-water temperature differences shown in Figure 12 in the time period 09:45-11:00 do not lead to large measured line widths in Figure 21 (10:05-11:18), we conclude that in this time interval the backup air temperature measuring thermometer was subject to localized heating and thus was not measuring the true temperature of the air above the ocean. From the graph of wind speed vs. time we note that, with the exception of a brief burst at 10:30, the air speed was less than 1 m./sec. in this time interval.

In Figure 22 (11:30-12:15) the line widths recorded appear to fall in the region of the minimum possible with the instrumentation, with the possible exception of the 30.6 micron line width obtained at a target range of 5000 m. at 11:30. Generally, the line width values computed theoretically appear to be unduly high. Again, this may be the result of the low wind speed, 1.3 m./sec.

In Figure 23 (12:35-14:00) the wind had stabilized at 2.5 to 3.5 m./sec., but the measured air-water difference values were from 1/2 to 1°C too high to permit agreement of measured and computed line width values.

The measured and computed line width values shown on Figure 24 (excluding the datum at 500 m.) show reasonable agreement. Although the theoretical values are based on only one meteorological measurement set, the 14:30 recording, the wind and temperature had stabilized by this time. Thus, the extrapolation of meteorological data to 15:00 seems justified.

We assume that the results of Figures 23 and 24 are based on reasonably correct data and uniform ambient conditions. Then the combined ratio of measured/computed line widths for the figures is $(0.61 \times 1.)^{1/2} = 0.78$.

VIII. GENERAL CONCLUSIONS

For strong turbulence with unstable atmospheric equilibrium, mean measured line widths will match the values computed from bulk meteorological measurements by the formulations given in this monograph to within a few percent. Single line width measurements can differ from the computed values by a factor of up to two times.

With neutral or weakly stable atmospheric conditions ($C_n^2 < 10^{-14}$ $m.^{2/3}$), minimum line width values varying from 3.5 to 4 arc sec. were recorded, rather than the stable 2.5 arc sec. line width expected. This seriously limited the accuracy with which results could be related to computed line width values, and thus the accuracy with which the effects of the turbulence could be inferred. Two sets of mean line widths obtained under atmospherically stable conditions gave combined ratios of measured to computed line widths of 0.78/1.0, but the turbulence contributions to the line widths were too small to draw conclusions about the accuracy of the theoretical turbulence formulations.

REFERENCES

1. W. E. K. Middleton, "Vision Through the Atmosphere," Univ. of Toronto Press, 1952, Sections 4.1 to 4.4.

2. K. Davison, T. Houlihan, C. Fairall, and G. Schacher, "Observations of the Temperature Structure Function Parameter, C_T^2, Over the Ocean," Report No. NPS63-78-005, Naval Postgraduate School, Monterey, CA 93940, September 1978 -- See extensive references in this report.

3. F. Replogle, Jr., "Measurements of the Effect of Refractive Irregularities in the Atmosphere on Imaging," TM No. 771196 Naval Underwater Systems Center, New London, CT 06320, 3 October 1977.

4. K. L. Davison, et alia, "Verification of the Bulk Method for Calculating Overwater Optical Turbulence," Applied Optics 20, No. 17, pp. 2919-2924, 1 September 1981.

5. R. Lutomirski and H. Yura, "Wave Structure Function and Mutual Coherence Function of an Optical Wave in a Turbulent Atmosphere," Jour. of Optical Soc. of America. 61, No. 4, p. 482, Equation (9b).

6. R. Lutomirski, et alia, "Degradation of Laser Systems by Atmospheric Turbulence," Report No. R-1171-ARPA/RC, June 1973, Equation (7.20).

7. H. Yura, "Short-term Average Optical-beam Spread in a Turbulent Medium," J.O.S.A. 63, No. 5, p. 567, May 1973, Equations (9) to (14).

APPENDIX I

COMPUTATION OF $C_n^2(z)$ FROM BULK METEOROLOGICAL MEASUREMENTS

From initial bulk meteorological measurements made at a height z' we proceed to derive $C_n^2(z)$, where z is any height above the surface. This will be done for both stable and unstable atmospheres.

The first variable to be obtained is the surface roughness distance z_0 given by

$$z_0 = 10 \exp(-0.35/\sqrt{C_{DN}}),$$

where C_{DN} is obtained from the wind speed U at z' from the tabulation

$C_{DN} \times 1000$	U(m/s)
$1.080\ U^{-0.15}$	0.3 to 2.2
0.770 + .086U	2.2 to 5.0
0.870 + .067U	5.0 to 8.0
1.200 + 0.25U	8.0 to 25.0

This leads to values of the drag coefficient C_{DN},

$$C_{DN}(U) = [0.35/\ln(z'/z_0)]^2. \qquad \text{(A-1)}$$

We then calculated a stability correction factor ξ_0', which is used in setting up scalar profiles of wind speed, temperature, and humidity. This is given by

$$\xi_0' = \frac{1.62z' \cdot (\Delta\theta + 6.2\times10^{-4} T\Delta_q)}{T \cdot \ln(5\times10^{-4} z') \cdot C_{DN}(U) \cdot U^2} \qquad \text{(A-2)}$$

where the variables are measured at height z'.

From the stability correction factor the true atmospheric stability at height z' is given implicitly by

$$\xi' = z'/L = \xi_0' \cdot \frac{[1-\psi_1(\xi')/\ln(z'/z_0)]^2}{1-\psi_2(\xi')/\ln(5\times10^4 z')}. \qquad \text{(A-3a)}$$

For <u>stable</u> atmospheric conditions ($\xi_0' > 0$),

$$\psi_1(\xi') = -4.7\xi'$$

and (A-3b)

$$\psi_2(\xi') = -6.5\xi',$$

and for unstable atmospheric conditions ($\xi'_0 < 0$),

$$\psi_1(\xi') = 2\ \ln[(1 + x)/2] + \ln[(1 + x^2)/2] - 2\ \tan^{-1}(x) + \pi/2,$$

with

$$x = (1 - 15\xi')^{1/4}$$

and (A-3c)

$$\psi_2(\xi') = 2\ \ln\ [(1 + \sqrt{1 - 9\xi'})/2]$$

For a stable atmosphere, Equations (A-3a) and (A-3b) may be formulated as a quadratic function of $\xi'(z')$ and solved for ξ'. For an unstable atmosphere Equations (A-3a) and (A-3c) may be solved iteratively for ξ' by substituting first ξ'_0 and then successively more accurate values of ξ' in the right hand side of Eq. (A-3a) and calculating the resulting improved value of ξ' after each substitution.

We now require values for the temperature and humidity scaling parameters, $T*$ and $Q*$ (gm/m^3), respectively. They are given by

$$T* = 0.47\Delta\theta/[\ln(5 \times 10^4 z') - \psi_2(\xi')] \qquad (A\text{-}4)$$

and

$$Q* = 1.3\ q* = 0.61\ \Delta q/[\ln(5 \times 10^4 z') - \psi_2(\xi')] \qquad (A\text{-}5)$$

From this point on we refer to the height z at which the turbulence will be observed. Then the stability parameter

$$\xi(z) = z/L = \frac{z}{z'} \cdot \xi'(z) \cdot \qquad (A\text{-}6)$$

From initial temperature and humidity difference data and the derived value of ξ we may now calculate structure functions for temperature and humidity, as well as the temperature-humidity covariance function. These are given by

$$C_T^2 = T_*^2 \cdot z^{-2/3} \cdot f(\xi), \qquad (A\text{-}7a)$$

$$C_Q^2 = 0.6\ Q_*^2 \cdot z^{-2/3} \cdot f(\xi), \qquad (A\text{-}7b)$$

$$C_{TQ} = 0.62\ T_* Q_* \cdot z^{-2/3} \cdot f(\xi), \qquad (A\text{-}7c)$$

where the height dependence function f is given for a stable atmosphere by

$$f(\xi)_s = 4.9\ (1 + 2.4\xi^{2/3})$$

and for an unstable atmosphere by

$$f(\xi)_u = 4.9\ (1 - 7\xi)^{-2/3}\ .$$

Finally, by combining the effects of temperature and humidity and relating these to variations in optical index, we obtain for the index structure function

$$C_n^2 = (79 \times 10^{-6} P/T^2)^2 \cdot (C_T^2 + 0.113\ C_{TQ} + 0.0031\ C_Q^2), \qquad \text{(A-8)}$$

where P is the air pressure in mb and T is the absolute air temperature.

For an optical path having a varying height above the sea surface, it is useful to have an expression for C_n^2 giving an explicit height dependence. Combining Equations (A-6), (A-7), and (A-8) gives

$$C_n^2 = (79 \times 10^{-6} P/T^2)^2 \cdot \left[T_*^2 + 0.070\ T_* Q_* + 0.0019\ Q_*^2\right] z^{-2/3} \cdot f(z/L). \qquad \text{(A-9)}$$

TM No. 821008
Prediction of Optical Image Quality Near
the Sea Surface from Meteorological Measurements
Frank S. Replogle, Jr.
Electromagnetic and Electro-Optics Sensors Division
Unclassified

DISTRIBUTION LIST

External:

CNO OP 009E, C. L. Heidler
OP 224C, Cdr. Cogsdell

NAVSEA 6111 Carl Campbell

NPS Dr. E. Crittenden
Dr. K. L. Davidson
Dr. C. W. Fairall

ONR Dr. David Lewis
Dr. Paul Twitchell

NASC Code 370C, Murray Schefer

NAVELEX PME107, E. Walsh

Naval Avionics Facility, James Russell

DDC

Internal:

Code	10	(Dr. W. A. Von Winkle)
	101	(Dr. E. S. Eby)
	101	(Dr. A. J. Van Woerkom)
	342	(D. McQueeney)
	3422	(F. S. Replogle, Jr.) (3 cys)
	3492	(C. M. Floyd)
	3821	(Dr. J. R. Short)
	4523	(3 cys)
	4533	
	45132	(10 cys)
	452	

External Copies: 12
Internal Copies: 24

Total 36

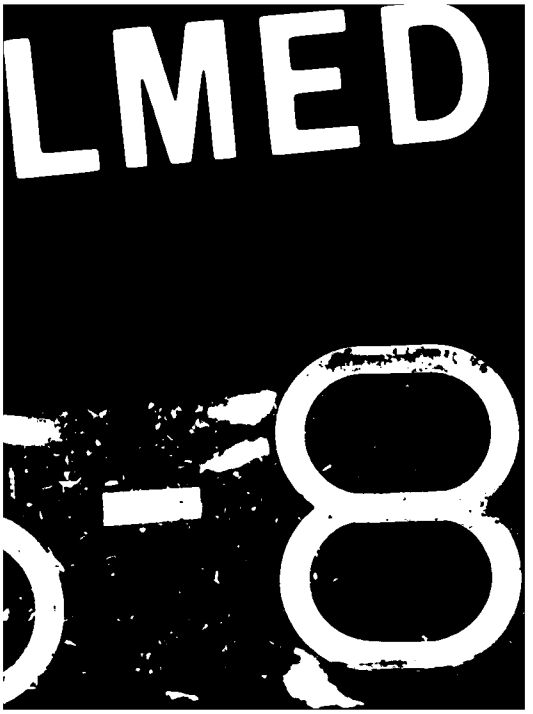
LMED